# The copBL operon protects Staphylococcus aureus from copper toxicity: CopL is an extracellular membrane-associated copper-binding protein

**Article** *in* Journal of Biological Chemistry · January 2019

DOI: 10.1074/jbc.RA118.004723



**9 authors**, including:

Zuelay Rosario
Rutgers, The State University of New Jersey
**5** PUBLICATIONS **147** CITATIONS

SEE PROFILE

Alexander Eletsky
University of Georgia
**49** PUBLICATIONS **2,106** CITATIONS

SEE PROFILE

Hassan Mohammed Al-Tameemi
University of Basrah
**12** PUBLICATIONS **93** CITATIONS

SEE PROFILE

G.V.T. Swapna
Rutgers, The State University of New Jersey
**72** PUBLICATIONS **2,083** CITATIONS

SEE PROFILE

# The *copBL* operon protects *Staphylococcus aureus* from copper toxicity: CopL is an extracellular membrane-associated copper-binding protein

**Zuelay Rosario-Cruz[1], Alexander Eletsky[3†], Nourhan S. Daigham[2], Hassan Al-Tameemi[1], G.V.T. Swapna[2], Peter C. Kahn[1], Thomas Szyperski[3], Gaetano T. Montelione[2,4,] *, and Jeffrey M. Boyd[1]***

[1]Department of Biochemistry and Microbiology, Rutgers, The State University of New Jersey, New Brunswick, New Jersey, 08901
[2] Department of Molecular Biology and Biochemistry, Center for Advanced Biotechnology and Medicine, and Northeast Structural Genomics Consortium, Rutgers, The State University of New Jersey, Piscataway, NJ 08854
[3]Department of Chemistry, The State University of New York at Buffalo and Northeast Structural Genomics Consortium, Buffalo, New York 14260
[4]Department of Biochemistry and Molecular Biology, Robert Wood Johnson Medical School, Rutgers The State University of New Jersey, Piscataway, NJ 08854
[†]Present address: Complex Carbohydrate Research Center, University of Georgia, Athens, Georgia, 30602

Running Title: *CopBL and copper homeostasis*

*To whom correspondence may be addressed: Jeffrey M. Boyd, Department of Biochemistry and Microbiology, 76 Lipman Drive, New Brunswick, New Jersey, 08901, Telephone: (848) 932-5604, E-mail: jeffboyd@SEBS.rutgers.edu. Gaetano T. Montelione, Department of Molecular Biology and Biochemistry, 679 Hoes Lane, Piscataway, New Jersey, 08854, Telephone: (848) 445-9868, E-mail: gtm@rutgers.edu

**Keywords**: copper, lipoprotein, metal, metal homeostasis, *Staphylococcus aureus*, MRSA, structural biology, virulence, redox homeostasis, arginine catabolic mobile element (ACME)

## ABSTRACT

As complications associated with antibiotic resistance have intensified, copper (Cu) is attracting attention as an antimicrobial agent. Recent studies have shown that copper surfaces decrease microbial burden, and host macrophages use Cu to increase bacterial killing. Not surprisingly, microbes have evolved mechanisms to tightly control intracellular Cu pools and protect against Cu toxicity. Here, we identified two genes (*copB* and *copL*) encoded within the *Staphylococcus aureus* arginine-catabolic mobile element (ACME) that we hypothesized function in Cu homeostasis. Supporting this hypothesis, mutational inactivation of *copB* or *copL* increased copper sensitivity. We found that *copBL* are co-transcribed and that their transcription is increased during copper stress and in a strain in which *csoR*, encoding a Cu-responsive transcriptional repressor, was mutated. Moreover, *copB* displayed genetic synergy with *copA,* suggesting that CopB functions in Cu export. We further observed that CopL functions independently of CopB or CopA in Cu toxicity protection and that CopL from the *S. aureus* clone USA300 is a membrane-bound and surface-exposed lipoprotein that binds up to four $Cu^{+}$ ions. Solution NMR structures of the homologous *Bacillus subtilis* CopL, together with phylogenetic analysis and chemical-shift perturbation experiments, identified conserved residues potentially involved in $Cu^{+}$ coordination. The solution NMR structure also revealed a novel Cu-binding architecture. Of note, a CopL variant with defective $Cu^{+}$ binding did not protect against Cu toxicity *in vivo*. Taken together, these findings indicate that the ACME-encoded CopB and CopL proteins are additional factors utilized by the highly successful *S. aureus* USA300 clone to suppress copper toxicity.

Because of its ability to cycle between its reduced ($Cu^{1+}$) and oxidized ($Cu^{2+}$) states, copper (Cu) has catalytic roles in metalloenzymes such as dioxygen reductases (1), superoxide dismutases (2), laccases (3), and several proteins involved in denitrification (4). Cu can also have non-redox structural roles, such as in transcription factors (5). Despite its necessity, intracellular Cu accumulation is toxic due to, in part, its ability to compete with other transition metals. Cu can displace iron from iron-sulfur (FeS) clusters leading to cluster destruction and protein inactivation, as well as inhibit the assembly of FeS clusters by binding to assembly proteins that would typically bind FeS clusters (6-9). Cu poisoning may also occur as a result of Fenton-type chemistry, in which $Cu^{1+}$ reacts with hydrogen peroxide leading to the formation of hydroxyl radicals (10), which in turn can damage proteins, membrane lipids, and DNA.

Copper has been used to sterilize wounds and drinking water and recently by hospitals to reduce microbial burden on touch surfaces (11,12). The human innate immune system uses Cu to kill invading microorganisms. Upon challenge with bacteria, macrophages accumulate Cu within phagosomes, where it may synergize with reactive oxygen species produced by NADPH oxidase to increase killing (13,14).

*Staphylococcus aureus* is a public health concern worldwide. *S. aureus* causes numerous infection types ranging from skin and soft tissue infections to more severe and life-threatening diseases, such as pneumonia, osteomyelitis, and bacteremia (15,16). Methicillin-resistant *S. aureus* (MRSA) infections have become more prevalent in community settings and this epidemic is widely attributed to the spread of the USA300 clone (17,18).

The genome of the USA300 clone has various mobile genetic elements, including the arginine catabolic mobile element (ACME) (19), which occupies a 31-kb region located adjacent to the SCC*mec*IV genetic element. Genes encoded within ACME provide an increased fitness advantage facilitating colonization and persistence of *S. aureus* on human skin. The ACME encoded arginine-deiminase system (*arc*) improves survival in acidic conditions (20) and the *speG* gene product provides resistance to high levels of host-derived polyamines (20,21).

Like other pathogens, *S. aureus* must employ strategies to tightly control intracellular Cu levels and avoid Cu toxicity. Membrane-spanning Cu exporters (22,23), Cu chaperons (24), and intracellular metallothioneins (25) are the most common defense mechanisms employed by microorganisms. The low molecular weight (LMW) thiols bacillithiol and glutathione can bind to Cu with relatively high affinity (26,27) and mutant strains lacking these compounds display sensitivity to copper suggesting potential role(s) for LMW thiols in Cu buffering (28,29).

In *S. aureus*, the Cu-sensitive operon repressor (CsoR) binds intracellular Cu leading to derepression of the *copAZ* operon (30). CopA is a transmembrane $P_{1B-1}$-type ATPase Cu exporter (31) and CopZ is a cytoplasmic Atx1-like Cu-binding chaperon (32). Some *S. aureus* strains have an additional predicted $P_{1B-3}$-subtype Cu transporter (CopB) and a Cu-dependent multicopper oxidase (Mco) (33). The described *copB* and *mco* genes are co-localized and located on mobile DNA in *S. aureus* (34). The *copBmco* genes provide increased Cu resistance and, like the *copAZ* operon, their transcription is regulated by CsoR (33,34). The function of Mco is currently unknown (35).

In the present work, we characterized the *copBL* operon located within the ACME region of the *S. aureus* USA300 clone, which encodes an additional Cu homeostatic mechanism. *copL* encodes for a membrane-bound, surface-exposed Cu-binding lipoprotein, and genetic evidence suggests that *copB* encodes a Cu exporter. The solution NMR structure of a *B. subtilis* CopL revealed that CopL has a unique Cu-binding architecture.

## RESULTS

*Analyses of* S. aureus *genes involved in copper homeostasis*. We analyzed the genome of the community-associated (CA)-MRSA strain USA300_FPR3757 (19) for genes involved in Cu homeostasis. We noted the presence of *csoR*, *copA*, and *copZ*. Further analysis identified the SAUSA300_0078 locus (CopB; **Figure 1A**), which shows 36% identity with CopA. CopB contains most of the conserved structural elements of $P_{1B}$-ATPases (**Figure S1**) including a phosphatase domain (TGES), a conserved CPX metal-binding sequence, and an ATP-binding domain (MXGDGXNDXP) (36). Unlike CopA, CopB lacks the N-terminal metal-binding CXXC motifs, but instead contains a His-rich N-terminus (**Figure S2**). The CopB described herein shares 85% and 56% identity to the previously described *S. aureus* CopB (33) and *Enterococcus hirae* CopB (37), respectively. The N-terminal metal binding domain of the CopB described herein is 52% and 42% identical to those of the N-terminal metal binding domains the previously described *S. aureus* CopB (33) and *Enterococcus hirae* CopB (37), respectively. A sequence alignment of the N-terminal metal binding domains of these proteins found that they vary in the number of amino acids and in histidine content (**Figure S2**).

A second open reading frame (ORF) is located 17-base-pairs (bp) downstream of *copB*. This ORF, which we and others named *copL* (copper-binding lipoprotein), encodes a putative lipoprotein containing two DUF1541 domains

(38). The *copBL* genes are located within the ACME region.

We identified ~200 CopL-like proteins in other microorganisms with the majority belonging to the *Actinobacteria* and *Firmicutes* phyla. The genomes containing *copL* also encoded for at least one additional Cu detoxification protein (CopA, CopZ, or CopB) (**Table S1**). The *copL* homologues are often co-localized near genes or within apparent operons encoding for genes involved in Cu homeostasis. *copL* is also located adjacent to *copB* in other staphylococci (**Figure S3**).

S. aureus *strains lacking CopB or CopL have increased sensitivity to Cu.* We tested the hypothesis that CopB and CopL function in Cu homeostasis. We constructed Δ*copB* and Δ*copL* mutants in the *S. aureus* strain USA300_LAC (WT) (**Figure S4**), which differs from the *S. aureus* strain USA300_FPR3757 by a few SNPs (39). The WT, Δ*copB*, and Δ*copL* strains were spot plated on chemically defined media containing varying concentrations of Cu. The Δ*copB* and Δ*copL* strains displayed decreased survival when cultured in the presence of Cu, but no growth abnormalities in the absence of Cu (**Figure 1B**). Genetic complementation verified that mutational inactivation of *copB* or *copL* was resulting in the observed growth defects (**Figure 1B**).

The *S. aureus* USA400 strain MW2 lacks *copB* and *copL*. We mobilized *copB* and *copL* to the MW2 strain via plasmid and examined Cu sensitivity. The MW2 strain containing *copB* or *copL* displayed increased resistance to Cu (**Figure 1C**). Expression of *copL* in the *S. aureus* strains Newman, COL, and RN4220 also resulted in increased Cu resistance (**Figure S5**).

*Strains lacking CopB or CopL display exacerbated phenotypes in cells unable to export cytoplasmic Cu via CopA*. We investigated whether CopB and CopL had a functional overlap with other genes involved in Cu homeostasis. Genes encoding proteins with functional overlap often display synergistic phenotypes when the gene products are absent or non-functional (40). An *S. aureus copA* mutant accumulates intracellular Cu and displays sensitivity to Cu (31). The *copA::Tn* and Δ*copB* mutants had decreased growth on solid media containing > 50 μM Cu, but no sensitivity was observed at lower (10 μM) Cu concentrations (**Figure 2A**). The phenotypes associated with the *copA::Tn* Δ*copB* mutations were synergistic for Cu sensitivity (**Figure 2A**). Similarly, the *copA::Tn* Δ*copL* double mutant strain was more sensitive to Cu than the *copA::Tn* and Δ*copL* single mutants (**Figure 2B**). The *copA::Tn* Δ*copB* Δ*copL* triple mutant was more sensitive to Cu than the *copA::Tn* Δ*copB* double mutant strain (**Figure 2C**).

The *S. aureus copZ::Tn* mutant did not display a Cu sensitivity phenotype on solid media (data not shown). The *copZ::Tn* Δ*copB* and *copZ::Tn* Δ*copL* strains displayed Cu sensitivity phenotypes similar to the Δ*copB* and Δ*copL* single mutants (data not shown).

Collectively, these results suggest that (a) CopA and CopB have a functional overlap and serve as Cu exporters, (b) CopL functions in Cu homeostasis independently of CopA and CopB, and (c) CopZ is not required to protect against Cu toxicity under the conditions examined.

copBL *transcription increases in the presence of Cu*. We tested the hypothesis that transcription of *copB* and *copL* increases in response to Cu. The abundances of the *copB* and *copL* transcripts were monitored in the WT strain grown with and without Cu. The *S. aureus copA* is induced during Cu stress (31,33); therefore, we quantified abundance of the *copA* transcript as a control. The transcripts of *copB* and *copL* were increased ~4-fold upon Cu stress, whereas the *copA* transcript was increased ~8-fold (**Figure 3A**).

We tested the hypothesis that *copB* and *copL* are co-transcribed. RNA was isolated from WT cultures grown in the presence of Cu and cDNA libraries were generated. Using cDNA as a PCR template, and primers nested within *copB* and *copL*, we were able to obtain an amplicon that spanned *copB* and *copL* (**Figure 3B**). No PCR products were obtained from control reactions lacking reverse transcriptase (-RT), confirming that the amplicon was not the result of genomic DNA contamination.

We created a transcriptional reporter to further analyze the regulation of *copB*. Transcriptional activity of *copB* increased in synchrony with the concentration of Cu added to the growth medium verifying the functionality of the reporter (**Figure 3C**). Transcriptional activity of *copB* did not increase upon challenge with $Mn^{2+}$, $Fe^{2+}$, $Zn^{2+}$, or $Co^{2+}$ (**Figure 3D**). In addition, the Δ*copB* and Δ*copL* mutant strains did not display increased sensitivity to these metals at concentrations that decreased the survival of the WT strain (data not shown).

*CsoR regulates the* copBL *operon*. We tested the hypothesis that CsoR regulates the *copBL* operon. CsoR binding sites have been identified in the promoters of *copZA* in *Bacillus subtilis* (41) and *copAZ* in *S. aureus* strain Newman (30), which are characterized by a pseudo-inverted repeat (TACCNNNN-GGGGGTA) (**Figure 4A)**. We analyzed the promoter region of the *copBL* in strain FPR3757 and found that it contains a putative CsoR binding site ~100-bp upstream of the translational start site.

We monitored the transcriptional activity of *copB* in the WT and *csoR::Tn* strains. The transcriptional activity of *copB* was increased in the *csoR::Tn* strain, suggesting that transcription of the *copBL* operon is repressed by CsoR (**Figure 4B**). Addition of Cu led to increased *copB* transcriptional activity in the WT strain, but not in the *csoR::Tn* strain (**Figure 4B**). The *S. aureus* strain Newman lacks the *copBL* operon, however the transcriptional activity of *copB* was also increased in an *S. aureus* Newman Δ*csoR* mutant when compared to the parent strain (**Figure S6**).

*CopL is membrane-associated and surface-exposed*. We tested the hypothesis that CopL is a surface exposed lipoprotein. We conducted cell fractionation experiments to verify the cellular location of CopL. We utilized a C-terminal FLAG-tagged *copL* that was under the transcriptional control of a xylose inducible promoter (*xylRO*) (pEPSA5_*copL*-FLAG). The *copL*-FLAG allele genetically complemented the Cu sensitivity phenotype of the Δ*copL* mutant strain, verifying the functionality of the fusion (data not shown). Cultures of the Δ*copL* strain harboring either pEPSA5 or pEPSA5_*copL*-FLAG were grown in the presence and absence of xylose. Cells were fractionated into cytosolic and membrane fractions. CopL-FLAG was detected in whole cell extracts and membrane fractions, but not in cytosolic fractions (**Figure 5A**). CopL-FLAG was also detected in non-induced samples, albeit at a much lower intensity, which is likely the result of leaky expression. CopL-FLAG was not detected in cells containing only empty vector.

The TOPCONS algorithm (42) predicted that CopL contains an N-terminal membrane targeting signal-sequence (**Figure S1**), which is a characteristic of proteins that are translocated across the cytoplasmic membrane (43). The LipoP server (44) identified a lipobox motif (sequence: LSAC) that is processed to provide a covalent lipid-linked membrane anchor. Lipoproteins in gram-positive bacteria are anchored to the cytoplasmic membrane with the C-termini facing the extracellular surface (45). We examined whether the functionality of the CopL protein depends on its cellular localization. We cloned a *copL* allele lacking the membrane translocation signal-sequence and lipobox, which we refer to as the truncated CopL (CopL(T)), into pEPSA5 (**Figure 5B**). CopL(T) did not complement the Cu sensitivity phenotype of the Δ*copL* strain, whereas the full-length CopL did **(Figure 5B)**. Cellular fractionation experiments using the Δ*copL* strain containing pEPSA5_*copL*(T)-FLAG revealed that the CopL(T) accumulated in the soluble cytosolic fractions, but not in the membrane fraction (data not shown). These results suggested that CopL does not function to protect against Cu toxicity unless localized to the membrane.

Nuc2 is a surface-exposed nuclease anchored to the membrane via its signal peptide (46). We created constructs encoding for chimeric proteins in which CopL(T) was fused to either Nuc2 (pEPSA5_*nuc2*-*copL*) or the described Nuc2 signal sequence (pEPSA5_*nuc2*(SS)-*copL*) (**Figure 5C**). Both chimeric constructs genetically complemented the Cu sensitivity phenotype of the Δ*copL* strain (**Figure 5C**).

Altogether, the data in **Figure 5** suggested that CopL is membrane-associated, surface exposed, and requires membrane association to protect against Cu toxicity.

S. aureus *CopL (saCopL) binds copper in vitro.* We tested the hypothesis that saCopL is a Cu-binding protein. Recombinant soluble saCopL(T) was purified from *Escherichia coli* (**Figure S7**) and $Cu^{1+}$ binding was examined using ultraviolet (UV)-visible absorption spectroscopy. Titrating $Cu^{1+}$ into apo-saCopL(T) resulted in gradual increases of the absorbance in the UV region ($A_{243}$). The change of $A_{243}$ was plotted as a function of the $Cu^{1+}$ / saCopL(T) ratio (**Figure 6A**). The formation of $Cu^{1+}$-saCopL(T) was linear and reached saturation after the addition of ~4 molar equivalents of $Cu^{1+}$.

Competition experiments were conducted to determine the $Cu^{1+}$ binding affinity of saCopL(T). Bathocuprione disulfonate (BCS) forms a complex with $Cu^{1+}$ in a 2:1 ratio [$Cu^{1+}$-$(BCS)_2$] that has an absorption maximum at $A_{483nm}$ (47). To determine the effective $Cu^{1+}$ binding affinity of saCopL(T), $Cu^{1+}$ and BCS were combined anaerobically. A fixed concentration of saCopL(T) was then titrated into the sample and absorption spectra recorded. The formation of $Cu^{1+}$-saCopL(T) was determined by monitoring the decrease in absorbance ($A_{483nm}$) after each addition (**Figure 6B**).

At each of the saCopL(T) concentrations examined, Equation 6 of Xiao *et al.* enabled calculation of $K_d$ for the protein-copper complex (48). The calculation yields the product of $K_d$ and $\beta_2$, where $\beta_2$ is the association constant between copper and Bcs. We used $\beta_2 = 10^{19.8}$ (47) and the resulting $K_d$ value was $4.98 \pm 0.20 \times 10^{-18}$ M.

*Structure of B. subtilis CopL (bsCopL) reveals a novel Cu-binding motif. B. subtilis ydhK* (bs*copL*) encodes a homolog of *S. aureus* CopL, with sequence identity of ~63% in the C-terminal region (**Figure S8**). A *B. subtilis* Δ*copL* mutant was more sensitive to growth in the presence of Cu than the parent strain (**Figure S9**). As the unpublished 3D solution NMR structure of this homologous protein was already available from the NIH Protein Structure Initiative (49) structural bioinformatics efforts, we used these NMR assignments and structure to validate that CopL does in fact bind Cu and predict Cu binding ligands.

The solution NMR structure of the bsCopL fragment comprising residues 83-205, truncated to remove the signal peptide and lipobox motif, forms a well-ordered structure in solution (**Figure S10**), consisting of a pair of distorted β-barrels joined by two shared β-strands, and includes two short turns with a $3_{10}$-helix geometry (**Figures 7A and S10**). The β-strands (A-G) consist of residues 87-90, 102-118, 127-134, 135-137, 141-153, 166-184, 189-198 and 202-204, while the $3_{10}$-helical turns consist of residues 96-98 and 135-137. The two homologous DUF1541 domains are found to form a single structural unit, as each β-barrel is comprised of polypeptide segments from both DUF1541 domains. An unusual structural feature of bsCopL is the *cis* conformation of the peptide bonds between two conserved residue pairs, Lys131-Trp132 and Lys195-Trp196 (**Figure 7A**), which results in a stacked orientation of their side-chains. The strong sequential $H^\alpha$-$H^\alpha$ NOE peaks supporting the *cis* conformation of these two non-proline peptide bonds are presented in **Figure S11**.

Residue conservation scores mapped onto the bsCopL structure indicate that the most conserved surface region, at the interface of the two β-barrels (**Figures 7B, S12, and S13**), represents a likely binding site for copper atoms. Copper coordination in proteins is usually mediated by nitrogen atoms of histidine rings, and sulfur atoms of cysteines and methionines; in less common cases it involves side-chain oxygen atoms of aspartic and glutamic acids, glutamine, or tyrosine, backbone carbonyl oxygens, and even indole rings of tryptophan in the form of π-cation interactions (50,51). A search for conserved residues of this type yields His94, Met95, Met98, His129, His130, His158, Met159, Met162 and His194 (**Figure 7A**) as the most likely candidates. This is also consistent with the neutral ε1-protonated tautomer states of His94, His130, His158 and His194 side-chains (**Figure S14**). A potential contribution to Cu-binding may come from the backbone carbonyl oxygen atoms of Lys131 and Lys195, which are surface-exposed, and do not form intramolecular hydrogen bonds. These conserved residues do not appear to match any known type of protein copper center (50,51).

A search of PDB90 (non-redundant subset of the PDB database with proteins sharing less than 90% sequence identity) for similar protein structures using DALI (52) produced 27 significant protein chain hits (Z-score ≥ 5). However, 25 of those the aligned segments were only between 45 and 69 residues long, with sequence identities to bsCopL between 10% and 23% and Cα atom r.m.s.d. between 1.3 and 3.8 Å. Here, the matching segments corresponded to only a single β-barrel of bsCopL. For the remaining two proteins, PDB IDs 2QQR and 2MAM, the aligned segments were 82 and 91 residues long, respectively. Both are tandem tudor domain proteins of human origin, the former a histone demethylase and the latter a DNA-binding protein. However, the sequence identity to bsCopL was only 13% and 19%, respectively. Global Cα atom r.m.s.d. was quite high at 5.0 and 5.3 Å, due to a significantly different relative orientation of the β-barrels. None of the structurally similar proteins contained the conserved histidine and methionine residues of bsCopL. Accordingly, we conclude that bsCopL features a novel Cu-binding protein architecture.

*Backbone $^1H$, $^{15}N$ chemical shift perturbation study of bsCopL interaction with $Cu^{1+}$*. For $Cu^{1+}$-binding studies, the $His_6$ purification tag was removed by TEV protease cleavage. The resulting protein includes three extra residues (SHM) at the N-terminal end of the bsCopL sequence. The 2D [$^{15}$N, $^1$H] heteronuclear single-quantum correlation (HSQC) spectrum of bsCopL (residues 83-205) is shown in **Figure S15,** with backbone and side-chain resonance assignments [deposited in the Biological Magnetic Resonance Bank (BMRB ID 16942)]. Similar spectra were obtained upon addition of 1 mM EDTA (data not shown), demonstrating that under the conditions used for these NMR studies, no Cu or other related residual metal ions are associated with apo-bsCopL protein samples. The

[$^{15}$N-$^{1}$H]-HSQC spectra of the apo-bsCopL with the C-terminal hexa-His tag and apo-bsCopL prepared with no hexa-His tag are essentially identical, aside from the small spectral differences due to the N- and C-terminal regions (**Figure S16)**.

To confirm the ability of bsCopL to bind copper *in vitro*, and to identify the $Cu^{1+}$ binding sites, 8 mol/mol equivalents of $Cu^{1+}$ were added to the apo-bsCopL protein and the buffer was exchanged to remove adventitiously associated $Cu^{1+}$ ions. Sequence-specific backbone NMR resonance assignments were then determined using standard triple-resonance NMR experiments (Supplementary Table S3), and deposited in the Biological Magnetic Resonance Bank (BMRB ID 27741)

Comparison of the overlay of the assigned 2D [$^{15}$N,$^{1}$H]-HSQC spectra of apo-bsCopL and holo-bsCopL (**Figure 8**) revealed that $Cu^{1+}$ addition results in specific chemical shift perturbations. The numerous spectral changes induced upon copper addition unambiguously demonstrate $Cu^{1+}$ association with bsCopL. A plot of chemical shift perturbations along the protein sequence is shown in **Figure S17**. When mapped onto the 3D structure of *B. subtilis* apo-bsCopL (**Figure 9**), these data demonstrate that many residues with significant chemical shift perturbations are located in the conserved surface region at the interface of the two β-barrels, which, as outlined above, we predict based on amino acid composition and conservation to include copper-binding sites.

To further confirm reversible copper association, the $Cu^{1+}$ chelator BCS was added to the holo-bsCopL protein sample followed by recording a [$^{15}$N,$^{1}$H-]-HSQC spectrum. As expected, the spectrum of the BCS-treated sample almost fully returned to match that of the apo-bsCopL (**Figure S18**).

*A CopL variant with decreased Cu binding does not protect against Cu toxicity* in vivo. We tested the hypothesis that Cu binding by CopL is necessary to protect from Cu toxicity. We created a construct which encoded for a *S. aureus copL* mutant allele (called *copL**) that encoded for the following directed changes to CopL: H70A, M71A, H134A, and M135A (H94, M95, H158, and M159 in bsCopL) (**Figure 10A**). These are strictly conserved residues that NMR studies suggested may function in $Cu^{1+}$ ligation. The *copL** allele was unable to correct the Cu-dependent growth defects of a *S. aureus* Δ*copL* mutant (Figure 10A).

We purified saCopL(T)* (*viz*, [H70A, M71A, H134A, M135A]-CopL(T)) and examined the near UV circular dichroism spectra of the apo-saCopL(T) and apo-saCopL(T)* proteins. The spectra were nearly identical indicating little difference in secondary structure between the variants (**Figure S19**). We next titrated with $Cu^{1+}$ into saCopL(T)* and monitored spectral changes using UV absorption spectroscopy. $Cu^{1+}$ titration resulted in a linear increase in absorbance at 243 nm and the absorbance plateaued after approximately two equivalents of $Cu^{1+}$ per saCopL(T)* (**Figure 10B**). These data indicate that the saCopL(T)* variant binds less $Cu^{1+}$ than saCopL(T). We next titrated saCopL(T)* into a solution of BCS and $Cu^{1+}$ and monitored absorbance at 483 nm. The addition of saCopL(T)* decreased absorbance at 483 nm, but not to the extent of that of saCopL(T) (**Figure 10C**). saCopL(T)* binds $Cu^{1+}$ with a $K_d$ of 1.35 ± 0.17 x $10^{-17}$ M, which is approximately 3-fold lower than the affinity of saCopL(T) for $Cu^{1+}$.

## DISCUSSION

This study was initiated to further investigate the mechanisms of copper (Cu) homeostasis in the epidemic CA-MRSA *Staphylococcus aureus* USA300 clone. The work presented has re-affirmed the roles of CopA and CsoR in Cu efflux and intracellular Cu sensing, respectively. We have also assigned roles for *copB* and *copL* in Cu homeostasis. These data, as well as published work on CopA (31), CopZ (32), and CsoR (53), resulted in a working model for Cu homeostasis in the *S. aureus* USA300_LAC, which is illustrated in **Figure 11**. Upon sensing Cu in the cytosol, CsoR derepresses transcription of the *copAZ* and *copBL* operons. The binding of apo-CsoR to the *copB* promoter was recently confirmed by Purves et al (54). CopZ binds Cu and acts as an intracellular Cu buffer delivering it to CopA. The CopA and CopB proteins function to efflux Cu from the cytosol. CopL is a membrane-associated, surface-exposed protein that binds Cu on the outside of the cell preventing it from entering the cytosol and binds Cu after efflux by CopA or CopB.

CopL tightly binds $Cu^{1+}$ with dissociation constant of 4.98 ± 0.20 x $10^{-18}$ M. For comparison, the reported $Cu^{1+}$ binding affinities of the *S. aureus* (30), *B. subtilis* (55), and *Mycobacterium tuberculosis* (53) CsoR proteins, HAH1 from *homo sapiens* (56), and N-terminal metal binding domain of CopA (57) and CopZ from *B. subtilis* (58) are of the same order of magnitude as CopL. The CusCFBA system protects the *Escherichia coli* cytosol and periplasm from Cu (59). The metallochaperone of this system (CusF) has a $Cu^{1+}$ $K_d$ of 5.0 ± 1.2 x $10^{-15}$ M (60).

It should be emphasized that small differences in binding affinity among the individual CopL binding sites could exist, but this could not be confirmed by the present data. The $K_d$ values reported here should therefore be considered weighted averages of the sites. It is clear nevertheless that the binding is tight and comparable to that of other copper binding proteins. It is also clear (**Figure 10C**) that the CopL* variant binds copper with less affinity than the wild-type CopL.

One aim of the work presented was to validate that CopL, from both *S. aureas* or *B. subtilis,* bind $Cu^{1+}$. This was achieved using $Cu^{1+}$ binding data on *S. aureas* CopL, and NMR studies on the *B. subtilis* CopL. Although there may in fact be structural differences in the $Cu^{1+}$-binding networks of *S. aureas* and *B. subtilis* CopL, the basic residues in the $Cu^{1+}$-binding side of *B. subtilis* CopL form a highly conserved network that is common to other homologs of this domain family, including *S. aureas* CopL.

The solution NMR structure of bsCopL revealed a novel copper-binding architecture. The overall structure of $Cu^{1+}$-bound form is similar to that of the apo-form since most distant residues do not exhibit perturbations of chemical shifts upon $Cu^{1+}$-binding. In order to preserve these NMR data for more comprehensive future studies, we have deposited these chemical shift data in the BioMagRes Database (BMRB ID 27741).

The 3D structure of bsCopL(T) contains unusual *cis* peptide bonds between two conserved residue pairs, Lys131-Trp132 and Lys195-Trp196. Non-proline *cis* peptide bonds are rare and occur only in about 0.03% of all peptide bonds in known protein structures (61). Their occurrence is significantly more frequent in structures determined at high resolution than in structures determined at medium and low resolution, suggesting that these bonds may be more abundant than generally recognized (61). *Cis-trans* isomerization of peptide bonds before proline residues can play an important kinetic role in controlling protein folding (62,63). This isomerization can be catalyzed by enzymes known as prolyl-cis/trans isomerases which have been shown to act on X-Pro peptide bonds, but not non-proline peptide bonds (64). Non-proline *cis* peptide bonds tend to be buried and not greatly accessible compared to Xxx-Pro *cis* peptide bonds, which suggests that they may form early during the folding process (65). They tend to be observed near active sites indicating that they may sometimes be important for protein activity (61). The majority of the *cis* peptide bonds occur in regular secondary structures, more specifically in β-strands (65). In the case of bsCopL, the two non-Pro *cis* peptide bonds are located in β-strands β3 and β6, adjacent to the proposed Cu-binding residues H130 and H194, respectively. These *cis* peptide bond conformations result in unique local sidechain structure, with stacked orientation of their side-chains. Although there may be functional consequences of such non-Pro *cis* peptide bonds, such structure-function studies are difficult to carry out since mutations which prevent *cis* peptide bonds also tend to have structurally-disruptive effects.

The CA-MRSA epidemic is widely attributed to the spread of the USA300 clone (17,18). The majority of the genetic differences between USA300 and other staphylococcal strains of clinical importance are the presence of mobile genetic elements including ACME (19). Expression of the ACME-encoded arginine-deiminase system (*arc*) improves survival in acidic conditions (20) and the ACME-encoded *speG* gene provides resistance to high levels of host-derived polyamines and survival within murine abscesses (20,21,66).

While this manuscript was being revised, Purves et al. reported that *S. aureus* strains lacking *copB* (called *copX* in their study) or *copL* are sensitive to growth in the presence of Cu (54). Interestingly, they were not able to genetically complement the *copL* mutant and were only able to complement in the *copB* mutant in one of the two media utilized. They found that the *copB* or *copL* mutants, but not the *copA* mutant, had slightly increased cell associated Cu. The authors used these data to suggest a role for CopBL in Cu efflux. Similar to the findings reported herein, they found that CsoR controls transcription of the *copAZ* and *copBL* operons. They also reported that apo-CsoR binds to the *copB* promoter suggesting that it directly controls transcription of *copBL*. Importantly, Purves et al. showed that strains lacking CopB or CopL, but not a strain lacking CopA, had decreased survival in murine macrophages. These data highlight a potentially important roles of CopB and CopL in pathogenesis.

The human skin commensal *Staphylococcus epidermidis* contains the *copB, mco*, and *copL* genes in an apparent operon, as well as two additional Cu efflux proteins (67). Phylogenetic analyses suggest that the genes comprising ACME were assembled into a single genetic locus in *S. epidermidis* before they were transferred to *S. aureus*, which occurred prior to the epidemic expansion of the USA300 clone (66). Our bioinformatics analysis (**Table S1**) revealed that *S. xylosus*, *S. capitis*, and *S. haemolyticus*, which are skin commensals, also have *copB* and *copL*. The acquisition of genetic elements from species that share the same niche is a strategy employed by *S. aureus* to adapt to new environments (68,69). It is tempting to speculate that additional Cu detoxification mechanisms provided by the ACME-encoded *copBL* operon further promotes survival on skin; however, this speculation awaits further examination.

A USA300 Latin American variant (USA300-LV) has become one of the most prevalent clones associated to MRSA infections in community settings in South America. Most of the genomic differences between USA300-LV and USA300 can be attributed to mobile genetic elements, and specifically, to the absence of ACME in USA300-LV (70). Despite this difference, the USA300-LV genome contains *copBL*. Similar to the location of *copBL* in USA300, *copBL* in USA300-LV are located adjacent to SCC*mec* on a mobile genetic element, which has been designated as the copper and mercury resistance mobile element (COMER) (70).

Mobile genetic elements containing copper detoxification islands have been discovered in other organisms (71). Copper resistance mechanisms acquired via transposable elements include copper transporters, multicopper oxidases or, as reported in this study, membrane-bound lipoproteins. These studies provide additional evidence that copper exposure (immune system, healthcare settings, and/or diet) may not only promote the dissemination of genetic elements that result in the development of metal-resistant microorganisms, but also strains that are hyper-virulent and resistant to antimicrobials.

In summary, the work presented here describes an additional strategy by which *S. aureus* protects against copper toxicity. The ACME-encoded *copBL* may contribute to the high success of USA300, by providing protection from Cu-dependent killing. Moreover, the fact that *copBL* is encoded on mobile DNA alongside virulence factors suggests that the maintenance of Cu homeostasis could be a selective pressure for mobilization of alternate virulence factors or antibiotic resistance genes.

## EXPERIMENTAL PROCEDURES

*Reagents*. Restriction enzymes, quick DNA ligase kit, deoxynucleoside triphosphates, and Phusion DNA polymerase were purchased from New England Biolabs. Primers were obtained from Integrated DNA Technologies and listed in **Table S2**. Plasmid mini-prep and gel extraction kits were purchased from Qiagen. Lysostaphin was purchased from Ambi Products. Tryptic Soy Broth (TSB) was purchased from MP Biomedicals. The ELC chemiluminescent detection kit was purchased from Pierce. Pierce Protease and Phosphatase Inhibitor Mini Tablets were purchased from ThermoScientific. GSTrap 4B columns and PreScission Protease were purchased from GE Healthcare. Unless specified, all other chemicals were purchased from Sigma-Aldrich and were of the highest purity available.

*Bacterial Strains and Growth Conditions*. Bacterial strains used in this work are listed in **Table 1**. Unless otherwise noted, the *S. aureus* strains used in this study are derived from the community-associated MRSA USA300 LAC strain that was cured of the pUSA03 plasmid, which confers erythromycin resistance (72). *S. aureus* strains were cultured in TSB or a defined medium and *Escherichia coli* strains were grown in Luria Broth (LB). Unless otherwise specified, all bacterial strains were cultured at 37°C. The chemically defined medium was previously described (73) and contained: 1 g $(NH_4)_2SO_4$, 4.5 g $KH_2PO_4$, 10.5 g $K_2HPO_4$, 110 mM NaCl, 30 mM KCl, 50 µg nicotinic acid, 50 µg pantothenic acid, 50 µg thiamine, 0.3 µg biotin, and 2.5 mg of each of the twenty amino acids, per 100 mL. When supplemented to the media, chemicals were added at the following concentrations: 10-300 µM $CuSO_4$; 50-200 µM $Fe_2(NH_4)_2(SO_4)_2$; 5-200 µM CoCl; 10-300 µM $MnSO_4$; 10-300 µM $ZnSO_4$. When appropriate, antibiotics were added at the following concentrations: 150 µg $mL^{-1}$ ampicillin (Amp), 6 or 30 µg $mL^{-1}$ chloramphenicol (Cm) (defined or complex media, respectively), 10 µg $mL^{-1}$ erythromycin (Erm), 3 µg $mL^{-1}$ tetracycline (Tet), and 150 ng $mL^{-1}$ anhydrotetracycline (A-Tet). Overnight cultures were grown in 7 mL culture tubes containing 2 mL of TSB shaken at 200 rpm. When growing overnight cultures of strains containing pEPSA-derived plasmids, 2% xylose (wt/vol) was added to the media.

*Construction of Mutant Strains and Plasmids*. Chromosomal DNA from JMB1100 was used as the template for PCR reactions used in the construction of plasmids. All plasmids were isolated from *Escherichia coli* DH5α and transformed into electrocompetent *S. aureus* RN4220 using a standard protocol (74). Phage α80 was used for plasmid and chromosomal transductions (75). All bacterial strains and DNA constructs were verified by PCR, genetic complementation, or DNA sequencing prior to use. DNA sequencing was conducted by Genewiz (South Plainfield, NJ).

Mutational inactivation of the *S. aureus copB* and *copL* genes was achieved by chromosomal deletion to yield the Δ*copB*, Δ*copL*, and Δ*copBL* mutant strains as described previously (76). For the Δ*copB* mutant, upstream and downstream regions of the *copB* gene (SAUSA300_0078) were PCR amplified using the following primers: ZRC199 and ZRC200; ZRC164 and ZRC201. PCR products were gel purified and fused by PCR using the ZRC199 and ZRC201 primers. For the Δ*copL* mutant, upstream and downstream regions of *copL* (SAUSA300_0079) were PCR amplified using the following primers: ZRC166 and ZRC167; ZRC168 and ZRC169. PCR products were gel purified and fused by PCR using the ZRC166 and ZRC169 primers. For the Δ*copBL* double mutant, upstream and downstream regions of the *copBL* operon were PCR amplified using the following primers: ZRC185 and ZRC186; ZRC168 and ZRC169. PCR products were gel purified and fused by PCR using the ZRC185 and ZRC169 primers. The Δ*copB*, Δ*copL*, and Δ*copBL* PCR products were digested with EcoRI and SalI, and ligated into similarly digested pJB38 (77). The recombinant vectors were transformed into chemically competent *E. coli* DH5α. PCR was used to screen for *E. coli* colonies harboring the recombinant plasmids using ZRC196 and ZRC201 primers for pJB38_Δ*copB*; ZRC196 and ZRC169 for pJB38_Δ*copL*; and ZRC196 and ZRC169 for pJB38_Δ*copBcopL*. The plasmids were isolated and mobilized into RN4220 and subsequently JMB1100. Colonies that were Cm sensitive were screened using PCR for the double recombination event. The Δ*copB* mutant strain was verified using the ZRC139 and ZRC201 primers. The Δ*copL* and Δ*copBL* mutants were verified using the ZRC139 and ZRC169 primers.

The pTET plasmid was used to construct the *copA*::Tn(*tet*) and *csoR*::Tn(*tet*) in the USA300 LAC background by allelic exchange as previously described (78). Mutational inactivation was confirmed using PCR with the following primers: *copA*::Tn(*ermB*), *copA*::Tn(*tet*), and *copZ*::Tn(*ermB*) with ZRC133 and ZRC134; *csoR*::Tn(*ermB*) and *csoR*::Tn(*tet*) with ZRC153 and ZRC155.

For complementation and expression studies, genes were cloned into pEPSA5 (79). The ZRC146 and ZRC141 primers were used to PCR amplify the *copB* gene. The ZRC149 and ZRC150 primers were used to PCR amplify the full-length *copL*. The ZRC184 and ZRC150 primers were used to PCR amplify the truncated *copL*. PCR products were digested with BamHI and SalI and ligated into similarly digested pEPSA5 to yield pEPSA5_*copB*, pEPSA5_*copL*, and pEPSA_*copL*(T) vectors. Plasmid-containing strains were PCR verified, using the pEPSA5upveri and ZRC141 (pEPSA_*copB*), or pEPSA5upveri and ZRC150 [(pEPSA5_*copL* or pEPSA_*copL*(T)].

The pEPSA5_*copL*-FLAG and pEPSA5_*copL*(T)-FLAG vectors were constructed by using the ZRC149 - ZRC181 and ZRC ZRC184 – ZRC181, respectively. The inserts were digested with BamH1 and NheI, then ligated into similarly digested pEPSA5_CitB-FLAG (80). Strains containing the pEPSA5_*copL*-FLAG plasmid were PCR verified using the pEPSA5upveri and ZRC181 primers. The pGEX-6P-1_*copL* was constructed using the ZRC198 and ZRC178 primers. The PCR product was digested with BamH1 and Xho, and then ligated into similarly digested pGEX-6P-1(GE Healthcare). The pGEX-6P-1_*copL** was created using the pEPSA5_*nuc2*(SS)-*copL** as a PCR template for *copL**. The *copB* transcriptional reporter was created by amplifying the *copB* promoter using the ZRC139 and ZRC140 primers. The PCR product was digested with HindIII and KpnI and ligated into similarly digested pCM11 (81).

The pEPSA5_*nuc2*-*copL* and pEPSA5_*nuc2*(SS)-*copL* vectors were created by using yeast homologous recombination cloning (YRC) in *Saccharomyces cerevisiae* FY2 as previously described (82,83). The pEPSA5_CitB-FLAG vector was linearized with NheI. The amplicon for the pEPSA5_*nuc2*(FL)-*copL* was created using the following primer pairs: ZRC188 and ZRC189; ZRC191 and ZRC193. The amplicon for the pEPSA5_*nuc2*(SS)-*copL* was created using the following primer pairs: ZRC188 and ZRC190; ZRC192 and ZRC193. Strains containing the pEPSA5_*nuc2*-*copL* and pEPSA5_*nuc2*(SS)-*copL* plasmids were PCR verified using the ZRC188 and ZRC193 primers. The pEPSA5_*nuc2*(SS)-*copL** was created using YCC cloning as outlined above using the additional following primers: CblSDM1for, CblSDM1rev, CblSDM2for, and CblSDM2rev.

*qRT-PCR*. RNA isolation and quantitative real-time PCR were performed as previously described with a few modifications (84). The WT (JMB1100) strain was cultured overnight in TSB in biological triplicates. Cells were pelleted by centrifugation and resuspended in PBS before diluting 1:100 into chemically defined media without and with 100 µM Cu. Cells were harvested 6 hours post-inoculation (OD ~1, $A_{600}$) by centrifugation, treated with RNAProtect (Qiagen) for 10 min at room temperature, and stored at -80°C. Pellets were thawed and washed twice with 0.5 mL of lysis buffer (50 mM RNAse-free Tris, pH 8). Cells were lysed with 20 µg DNAse and 20 µg Lysostaphin for 30 minutes at 37°C. RNAs were isolated using TRIzol reagent (Ambion) as per manufacturers protocol. DNA was digested with the TURBO DNA-free kit (Ambion - Life Technologies) and RNA quantified using a Nanodrop (ND-1000) Spectrophotometer. cDNA libraries were constructed using isolated RNA as a template with High Capacity RNA-to-cDNA Kit (Applied Biosystems). *Power* SYBR Green PCR Master Mix (Applied Biosystems) was used to perform qRT-PCR in an Applied Biosystems StepOnePlus thermocycler. Data was analyzed using the ΔΔCt method. CopARTfwd and CopARTrev primers were used to detect *copA* transcripts; CopBRTfwd and CopBRTrev primers were used to detect *copB* transcripts; CblRTfwd and CblRTrev primers were used to detect *copL* transcripts. Transcripts corresponding to the 16s rRNA gene were detected with 16sfwdRT and 16srevRT primers. RT primers were designed using the Primer Express 3.0 software from Applied Biosystems.

*Transcriptional Reporter Assays.* Strains containing the pCM11-derived reporters were grown overnight in TSB-Erm. The overnight cultures (>16 hours) were pelleted and resuspended in PBS. Washed cells were subcultured into 5 mL of fresh chemically defined media (1:100) in 30 mL culture tubes with and without copper. Culture aliquots were periodically removed (200 µL) and culture optical density ($A_{590}$) and fluorescence was monitored using a Perkin Elmer HTS 7000 Plus Bio Assay Reader. GFP was excited at 485 nm and emission was read at 535 nm. Relative fluorescence units were normalized with respect to the culture optical density at each time point.

*Cell Fractionation.* Overnight cultures were diluted to 0.1 OD ($A_{600}$) in fresh TSB with Cm. Cultures were induced with 0 % or 0.2 % xylose at 1 OD ($A_{600}$), incubated for two additional hours, and harvested by centrifugation. Cultures were resuspended and washed with PBS. Cells were lysed (PBS with 10 µg DNAse, 10 µg Lysostaphin, Protease, and Phosphatase Inhibitor Mini Tablets) at 37°C for ~45 min. The cell fractionation protocol was followed as previously described with modifications (85). Cell lysates were spun for 10 min at (12,000 x *g*, 4°C) to remove unbroken cells and debris. Supernatants (whole cell, crude lysates) were spun at 100,000 × g for 2 hr at 4 °C in Beckman Polyallomer Centrifuge Tubes using a Beckman Optima TLX Ultracentrifuge and TLA 120.2 rotor. The resulting supernatant was saved as the cytoplasmic fraction. The pellet (crude membrane fraction) was resuspended in membrane buffer (100 mM Tris-HCl [pH 7.5], 100 mM NaCl, 10 mM $MgCl_2$, 10 % glycerol, 0.1 % SDS) to solubilize membrane proteins and spun at 100,000 × g for 2 hr at 4 °C to remove the detergent-insoluble material. Supernatants were saved as the membrane soluble fractions.

*Western Blot Analysis.* A total of 40 µg of total protein per sample were separated using a SDS-PAGE gel. Proteins were transferred to a PVDF membrane and incubated with mouse monoclonal anti-FLAG primary antibody (Sigma-Aldrich) (1:4000 dilution) and subsequently HRP conjugated secondary antibody (BioRad)(1:12000 dilution). The blots were developed using chemi-luminescent detection (Pierce) and scanned as TIFF images.

*Protein concentration determination.* Protein concentration was determined using a bicinchoninic acid assay modified for a 96-well plate (86) with bovine serum albumin as a protein standard. Apo-saCopL(T) concentrations were also estimated spectrophotometrically using $\varepsilon_{280}$ = 19,940 $M^{-1}$ $cm^{-1}$. Apo-bsCopL(T) concentrations were estimated spectrophotometrically using $\varepsilon_{280}$ = 18,450 $M^{-1}$ $cm^{-1}$.

*Recombinant saCopL(T) Expression and Purification. E. coli* BL21 DE3 containing pGEX-6P-1_*copL* or pGEX-6P-1_*copL** was cultured overnight in LB-Amp and used to inoculate 1L of 2x YT media (16 g tryptone, 10 g yeast extract, and 5 g NaCl, pH 7.0) to 0.1 OD ($A_{600}$). Cultures were grown shaking at 30°C, induced with 1 mM IPTG at 0.8 OD ($A_{600}$), and incubated for additional 4 hr. Cultures were harvested by centrifugation, resuspended in cold PBS, and stored at -80°C. For lysis, thawed cell pastes were passed through a French press three times, and cell lysates were clarified by centrifugation (15,000 × g for 30 min at 4°C). Cell extracts were loaded onto GSTrap 4B columns pre-equilibrated with binding buffer (PBS, pH 7.4) and then washed with 30 column volumes of binding buffer. The column was washed with PreScission cleavage buffer (50 mM Tris-HCl, 150 mM NaCl, 1 mM EDTA, 1 mM

DTT, pH 7.5) and then incubated overnight at 4°C with the PreScission Protease before eluting the recombinant protein with PreScission cleavage buffer. Fractions were analyzed for purity by SDS-PAGE. Protein was concentrated using YM-3 Centriplus Centrifugal Concentrators (Millipore). Circular dichroism spectra were recorded using an AVIV model 62A (Aviv Associates, Lakewood, NJ) spectropolarimeter.

*Copper Binding and BCS Competition Assays.* All biochemical assays were conducted under strict anaerobic conditions, either in a Coy anaerobic chamber (Grass Lake, MI) or using sealed cuvettes and Hamilton gas tight syringes. $Cu^{1+}$ binding was conducted as previously described (55). After purification, apo-saCopL(T) was transferred to the anaerobic chamber and buffer exchanged (buffer R: 50 mM MOPS, 50 mM NaCl, pH 7.4) using a PD-10 column (GE Healthcare), concentrated, and allowed to incubate overnight to establish anaerobiosis. A 0.5 mM CuCl stock was prepared anaerobically in 10 mM HCl, 1 M NaCl, and 1 mM ascorbic acid. For $Cu^{1+}$-binding assays, 12.5 μM saCopL(T) and 100 μM ascorbic acid in a total volume of 600 μL buffer R was placed in an anaerobic cuvette. The absorbance of the sample at 243 nm was determined using a Beckman-Coulter DU800 spectrophotometer after each 4 μL addition of 0.5 mM $Cu^{1+}$.

Competition assays with the $Cu^{1+}$ specific chelator bathocuproine disulfonate (BCS) were conducted as previously described (55). Anaerobic solutions containing 0.5 mM BCS, 20 μM $Cu^{1+}$, 0.2 mM ascorbic acid, 50 mM NaCl, 50 mM MOPS, pH 7.4, were combined in a 700 μL in a sealed gas-tight cuvette. A series of additions of 80 μM saCopL(T) in buffer R were added to the cuvette. After each addition, and a subsequent three min incubation, the absorbance at 483 nm was recorded using a Beckman-Coulter DU800 spectrophotometer. For dilution correction, experiments were also performed in an identical manner using only buffer R. BCS forms a complex with $Cu^{1+}$ in a 2:1 ratio [$Cu^{1+}$-$(BCS)_2$], which can be monitored by changes in absorbance at 483 nm with an overall association constant of $\beta_2 = 10^{19.8}$ (47).

*Recombinant expression and purification of bsCopL(T). B. subtilis* bsCopL(T) (NESG Target ID SR518) was cloned, expressed, and purified following the standard NESG protocols (87). Briefly, the construct SR518-83-205-21.8, containing the 83-205 residue fragment with a C-terminal affinity purification tag LEHHHHHH and an N-terminal methionine, was cloned into a pET21 (Novagen) derivative vector. *Escherichia coli* BL21 (DE3) pMGK cells, a rare codon-enhanced strain, were transformed with SR518-83-205-21.8, and cultured in MJ9 minimal media (92) with $^{15}$N-ammonium sulfate and/or $^{13}$C-glucose as sole nitrogen and carbon sources. Uniformly [$^{13}$C;$^{15}$N]-labeled CopL (CopL-NC) was purified using an AKTAxpress (GE Healthcare) based two-step protocol consisting of IMAC (HisTrap HP) and gel filtration (HiLoad 26/60 Superdex 75) chromatography. The final yield of purified CopL-NC (> 95% homogenous by SDS-PAGE; 15.4 kDa by MALDI-TOF mass spectrometry) was about 73 mg/L. The final sample of CopL-NC for structure determination with NMR spectroscopy was prepared at a concentration of 0.4 mM in 10 mM Tris-HCl buffer solution, pH 7.5, containing 5% $D_2O$, 100 mM NaCl, 5 mM DTT, 0.02% $NaN_3$, and proteinase inhibitors (Roche). A uniformly $^{15}$N- and 5% biosynthetically-directed fractionally $^{13}$C-labeled sample CopL-NC5 was prepared in the same manner using a mixture of 95% natural abundance and 5% U-$^{13}$C-glucose as a carbon source yielding the final concentration of 0.7 mM. NMR samples were prepared by exchange via spin columns into 10 mM Tris-HCl buffer at pH 7.5, containing 100 mM NaCl and 5% v/v $D_2O$, and concentrating to about 0.12 mM.

This material was used to produce anisotropic NMR samples, CopL-NC5-PEG and CopL-NC5-Pf1, by adding 4% (w/v) $C_{12}E_5$-PEG/hexanol at 1:1 molar ratio, or 12.5 mg/ml of Pf1 phage, respectively. For measurement of $^{15}$N-$^{1}$H residual dipolar couplings (RDCs) additional anisotropic NMR samples, CopL-NC5-PEG and CopL-NC5-Pf1, were prepared from CopL-NC5 material by adding 4% (w/v) $C_{12}E_5$-PEG/hexanol at 1:1 molar ratio, or 12.5 mg/ml of Pf1 phage (ASLA Biotech), respectively.

For Cu-binding studies the same gene fragment (residues 83-205) was cloned into a pET15 (Novagen) derivative vector, pET15TEV_NESG (88), yielding the construct SR518-83-205-TEV. The corresponding N-terminal $His_6$-fusion protein was expressed and purified as described above, with uniform $^{15}$N-enrichment. The $His_6$ purification tag was then removed by TEV protease cleavage, followed by IMAC (HisTrap HP) purification and gel filtration chromatography, as described elsewhere (89). The resulting protein includes three extra residues (SHM) at the N-terminal end of the bsCopL sequence.

To prepare the holo-bsCopL-N protein sample, CuCl was prepared anaerobically in 10 mM HCl, 1 M NaCl, and 1 mM ascorbic acid. 2

mol/mol equivalent of CuCl was added to 1.4 mL of uniformly $^{15}$N-enriched apo-bsCopL (0.11 mM), to prevent protein precipitation. The sample was then concentrated to approximately 0.1 mL and then diluted to 1.4 mL with 10 mM Tris-HCl buffer at pH 7.5, containing 100 mM NaCl and 1 mM ascorbic acid. This was repeated three times (8 equivalents of $Cu^{1+}$). Subsequently, the buffer of the sample was exchanged to remove any excess or adventitiously associated $Cu^{1+}$. The final sample was adjusted to contain 5% $D_2O$ in 500 uL (~0.25 mM). The BCS-treated sample holo-bsCopL-N-BCS was prepared by adding 1 mM anaerobically prepared BCS to the holo-bsCopL-N protein sample. All the above procedures were carried out at room temperature and under aerobic conditions using sealed NMR tubes (Wilmad Glass).

*NMR spectroscopy and structure determination of bsCopL.* NMR data acquisition was carried out on Bruker AVANCE 600, 700, 800 and 900 MHz, as well as Varian INOVA 600 and 750 MHz spectrometers, all equipped with cryogenic inverse-detected triple-resonance probes. All NMR experiments were carried out at 25°C and are summarized in **Table S3**. 1D $^{15}$N relaxation HSQC spectra were processed with VNMRJ 4.2A (Agilent Technologies) and integrated over the $^1$H range 10.0 – 8.5 ppm. $^{15}$N relaxation times $T_1$ = 740±30 ms and $T_2$ = 85±9 ms were extracted by fitting exponential decay curves. Rotational correlation time $\tau_c$ was calculated using the 'slow molecular tumbling' approximation of the complete relaxation equations (90):

$$\tau_c = \frac{1}{4\pi\nu_N}\sqrt{6\frac{T_1}{T_2} - 7}$$

where $\nu_N$ represents the $^{15}$N resonance frequency. The resulting $\tau_c$ value of 7 ns indicates that CopL-NC is monomeric in solution. This finding was confirmed by analytical gel-filtration (GE Healthcare) followed by static light scattering (Wyatt Technology).

2D and 3D NMR spectra were processed with TopSpin (Bruker BioSpin), NMRPipe (91), or PROSA (92). Visualization and analysis of NMR spectra was performed with the programs CARA (93), XEASY (94), and Sparky (95). Chemical shifts of $^1$H spins were referenced to internal DSS, while $^{13}$C and $^{13}$N chemical shift were referenced indirectly via their gyromagnetic ratios according to IUPAC recommendations (96). Sequence-specific assignments of backbone ($^1$H$^N$, $^{15}$N, $^{13}$CO, $^{13}$C$^\alpha$) and $^{13}$C$^\beta$ resonances were obtained in a semi-automated manner by analyzing HNCO, HN(CA)CO, CBCA(CO)NH and HNCACB peak lists with the program PINE (97). Side-chain resonance assignment was performed interactively in CARA using HBHA(CO)NH, (H)CCH-COSY, (H)CCH-TOCSY, and $^{15}$N,$^{13}$C-resolved [$^1$H,$^1$H]-NOESY (mixing time 70 ms) spectra 2D [$^{13}$C,$^1$H] constant-time HSQC of CopL-NC5 was used to obtain stereospecific resonance assignments of valine and leucine methyl groups (98). Protonation and tautomeric states of His side-chains were determined from long-range 2D [$^{15}$N,$^1$H] HSQC (99) revealing that His129 is positively charged, while His94, His130, His158 and His194 are N$^{\varepsilon 2}$-protonated. Chemical shifts, NOE peak lists, $^{15}$N-$^1$H RDCs, and time-domain NOESY data were deposited in the BioMagResBank (100) under accession number 16942.

$^1$H-$^1$H upper distance constraints for structure determination were obtained from 3D $^{15}$N,$^{13}$C-resolved [$^1$H,$^1$H]-NOESY. Constraints for φ and ψ dihedral angle constraints were derived from backbone chemical shifts using TALOS+ (101). Automated iterative NOE peak assignment and structure calculation was initially performed with AutoStructure 2.2.1 (102) and CYANA 3.0 (103) using dihedral angle constraints and stereospecific assignments of Val and Leu methyl groups. The resulting consensus NOE assignments were verified and corrected by interactive spectral analysis. Subsequently calculations were performed iteratively with CYANA, with iterations used to verify and complete resonance assignments, refine NOESY peak lists and optimize the distance calibration constants. Backbone $^{15}$N-$^1$H RDCs for two alignment media were determined from *J*-modulated spectra (104) and used as orientational constraints for the folded core at the later stages of refinement. The final 20 conformers out of 100 were further refined by restrained molecular dynamics in explicit water (105) using the program CNS 1.2 (106) with the PARAM19 force field.

The bsCopL structure was determined using 1,725 NOE-based conformation-restricting distance restraints, together with 130 restraints on backbone dihedral angle phi and psi based on chemical shift data, and an additional 164 $^{15}$N-$^1$H residual dipolar coupling measurements. These data include 15.4 distance restraints per residue, and 7.1 long-range distance restraints per residue. Structural statistics and global quality factors were computed with PSVS 1.4 (107) and are summarized in **Table S4**. The goodness-of-fit between the final ensemble of conformers and the NOESY peak lists (108) was calculated with RPF module of AutoStructure 2.2.1 (102). The NMR-derived structures are well-converged, and have structure quality scores, including model vs data metrics for back-calculated NOESY spectra and knowledge-based packing scores, typical of very high quality, accurate NMR structures. The resulting coordinates of bsCopL were deposited in the Protein Data Bank with PDB ID 2KY9.

The structural presentations of the protein were produced with the programs Molmol (109) and Pymol (110). Residue conservation analysis was performed with the ConSurf server (111). A total of 399 non-redundant proteins sequences with sequence identity between 35% and 95% were selected from the UniRef90 database after 3 iterations of CSI-BLAST search with E-value cutoff of 0.0001 by using *B. subtilis* fragment 83-205 as a query and aligned with MAFFT algorithm.

For $Cu^{1+}$ studies, the construct used did not include a C-terminal hexaHis tag, and incorporated two additional N-terminal residues, compared to the construct used for structure determination. Sequence-specific assignments of backbone ($^1H^N$, $^{15}N$, $^{13}CO$, $^{13}C^{\alpha}$) and $^{13}C^{\beta}$ resonances were obtained for $Cu^{1+}$-loaded holo-CopL by manual interactive analysis of HNCO, HNCA, HN(CO)CA, CBCA(CO)NH and HNCACB spectra. Chemical shift perturbations (absolute value) of $^1H$ and $^{15}N$ backbone amides, $\Delta\delta_{NH}$, were then calculated relative to the same construct of apo-CopL lacking the C-terminal hexaHis tag using the following equation (112):

$$|\Delta\delta_{HN}| = [(\Delta\delta_H)^2 + (\Delta\delta_N/6)^2]^{1/2}$$

where $\Delta\delta_H$ and $\Delta\delta_N$ are the chemical shift changes in the $^1H^N$ and $^{15}N$ dimensions, respectively.



**Acknowledgments**: This work was supported by Rutgers University, the Charles and Johanna Busch Foundation, the USDA MRF project NE-1028 (JMB), and as a Community Outreach Project of the NIH NIGMS Protein Structure Initiative, grant U54 GM094597 (GTM and TS). ZRC was supported by the James Macmillan Endowed Fellowship and Rutgers University. JMB is supported by NIAID award 1R01AI139100-01. ND and GTM were supported by the Jerome and Lorraine Aresty Chair Endowment and NIH grant R01 GM120574. TS was supported by NSF grant MCB-1615570. NMR instrumentation used in this work was supported in part by NIH shared instrumentation grant 1S10-OD018207. When the NMR data acquisition took place, Prof. T. Szyperski was a member of the New York Structural Biology Center; the Center is a STAR center supported by the New York Office of Science, Technology and Academic Research. 900 MHz spectrometer was purchased with the funds from NIH, and the Keck Foundation. We thank R. Xiao, D. Lee, C. Ciccosanti, S. Sahdev, and T.B. Acton for producing *B. subtilis* CopL constructs and protein samples, G. Liu for assistance in NMR studies, and H.-W. Lee and Prof J. H. Prestegard for providing RDC data. We also thank Prof. W. Belden and Prof. G. Zylstra for the use of their real-time thermocycler and spectrophotometer, respectively.

**Conflict of interest**: GTM is a founder of Nexomics Biosciences, Inc.

**Author contributions**: JMB and ZRC envisioned the project. GTM and TS developed the platform used here for NMR structure determination. ZRC, HAT, PCK, and JMB conducted the biological work shown. AE and TS determined the solution NMR structure of CopL. JMB, NSD, GVTS, and GTM prepared samples for NMR studies and carried out chemical shift perturbation analysis. ZRC, AE, NSD, GTM, and JMB wrote the manuscript.

## REFERENCES

1. Sousa, F. L., Alves, R. J., Ribeiro, M. A., Pereira-Leal, J. B., Teixeira, M., and Pereira, M. M. (2012) The superfamily of heme-copper oxygen reductases: types and evolutionary considerations. *Biochim Biophys Acta* **1817**, 629-637
2. Osman, D., Patterson, C. J., Bailey, K., Fisher, K., Robinson, N. J., Rigby, S. E., and Cavet, J. S. (2013) The copper supply pathway to a Salmonella Cu,Zn-superoxide dismutase (SodCII) involves P(1B)-type ATPase copper efflux and periplasmic CueP. *Mol Microbiol* **87**, 466-477

3. Claus, H. (2003) Laccases and their occurrence in prokaryotes. *Arch Microbiol* **179**, 145-150
4. Tavares, P., Pereira, A. S., Moura, J. J., and Moura, I. (2006) Metalloenzymes of the denitrification pathway. *Journal of inorganic biochemistry* **100**, 2087-2100
5. Rutherford, J. C., and Bird, A. J. (2004) Metal-responsive transcription factors that regulate iron, zinc, and copper homeostasis in eukaryotic cells. *Eukaryot Cell* **3**, 1-13
6. Macomber, L., and Imlay, J. A. (2009) The iron-sulfur clusters of dehydratases are primary intracellular targets of copper toxicity. *Proc Natl Acad Sci U S A* **106**, 8344-8349
7. Chillappagari, S., Seubert, A., Trip, H., Kuipers, O. P., Marahiel, M. A., and Miethke, M. (2010) Copper stress affects iron homeostasis by destabilizing iron-sulfur cluster formation in *Bacillus subtilis*. *J Bacteriol* **192**, 2512-2524
8. Fung, D. K., Lau, W. Y., Chan, W. T., and Yan, A. (2013) Copper efflux is induced during anaerobic amino acid limitation in *Escherichia coli* to protect iron-sulfur cluster enzymes and biogenesis. *J Bacteriol* **195**, 4556-4568
9. Tan, G., Cheng, Z., Pang, Y., Landry, A. P., Li, J., Lu, J., and Ding, H. (2014) Copper binding in IscA inhibits iron-sulphur cluster assembly in *Escherichia coli*. *Mol Microbiol* **93**, 629-644
10. Gunther, M. R., Hanna, P. M., Mason, R. P., and Cohen, M. S. (1995) Hydroxyl radical formation from cuprous ion and hydrogen peroxide: a spin-trapping study. *Arch Biochem Biophys* **316**, 515-522
11. Mikolay, A., Huggett, S., Tikana, L., Grass, G., Braun, J., and Nies, D. H. (2010) Survival of bacteria on metallic copper surfaces in a hospital trial. *Appl Microbiol Biotechnol* **87**, 1875-1879
12. Schmidt, M. G., Attaway, H. H., Sharpe, P. A., John, J., Jr., Sepkowitz, K. A., Morgan, A., Fairey, S. E., Singh, S., Steed, L. L., Cantey, J. R., Freeman, K. D., Michels, H. T., and Salgado, C. D. (2012) Sustained reduction of microbial burden on common hospital surfaces through introduction of copper. *J Clin Microbiol* **50**, 2217-2223
13. White, C., Lee, J., Kambe, T., Fritsche, K., and Petris, M. J. (2009) A role for the ATP7A copper-transporting ATPase in macrophage bactericidal activity. *J Biol Chem* **284**, 33949-33956
14. Achard, M. E., Stafford, S. L., Bokil, N. J., Chartres, J., Bernhardt, P. V., Schembri, M. A., Sweet, M. J., and McEwan, A. G. (2012) Copper redistribution in murine macrophages in response to *Salmonella* infection. *Biochem J* **444**, 51-57
15. Klevens, R. M., Morrison, M. A., Nadle, J., Petit, S., Gershman, K., Ray, S., Harrison, L. H., Lynfield, R., Dumyati, G., Townes, J. M., Craig, A. S., Zell, E. R., Fosheim, G. E., McDougal, L. K., Carey, R. B., and Fridkin, S. K. (2007) Invasive methicillin-resistant *Staphylococcus aureus* infections in the United States. *JAMA* **298**, 1763-1771
16. Otto, M. (2010) Basis of virulence in community-associated methicillin-resistant *Staphylococcus aureus*. *Annual review of microbiology* **64**, 143-162
17. Tenover, F. C., McDougal, L. K., Goering, R. V., Killgore, G., Projan, S. J., Patel, J. B., and Dunman, P. M. (2006) Characterization of a strain of community-associated methicillin-resistant *Staphylococcus aureus* widely disseminated in the United States. *J Clin Microbiol* **44**, 108-118
18. Talan, D. A., Krishnadasan, A., Gorwitz, R. J., Fosheim, G. E., Limbago, B., Albrecht, V., Moran, G. J., and Group, E. M. I. N. S. (2011) Comparison of Staphylococcus aureus from skin and soft-tissue infections in US emergency department patients, 2004 and 2008. *Clin Infect Dis* **53**, 144-149
19. Diep, B. A., Gill, S. R., Chang, R. F., Phan, T. H., Chen, J. H., Davidson, M. G., Lin, F., Lin, J., Carleton, H. A., Mongodin, E. F., Sensabaugh, G. F., and Perdreau-

Remington, F. (2006) Complete genome sequence of USA300, an epidemic clone of community-acquired meticillin-resistant *Staphylococcus aureus*. *Lancet* **367**, 731-739
20. Thurlow, L. R., Joshi, G. S., Clark, J. R., Spontak, J. S., Neely, C. J., Maile, R., and Richardson, A. R. (2013) Functional modularity of the arginine catabolic mobile element contributes to the success of USA300 methicillin-resistant *Staphylococcus aureus*. *Cell Host Microbe* **13**, 100-107
21. Joshi, G. S., Spontak, J. S., Klapper, D. G., and Richardson, A. R. (2011) Arginine catabolic mobile element encoded speG abrogates the unique hypersensitivity of *Staphylococcus aureus* to exogenous polyamines. *Mol Microbiol* **82**, 9-20
22. Arguello, J. M., Gonzalez-Guerrero, M., and Raimunda, D. (2011) Bacterial transition metal P(1B)-ATPases: transport mechanism and roles in virulence. *Biochemistry* **50**, 9940-9949
23. Arguello, J. M., Patel, S. J., and Quintana, J. (2016) Bacterial Cu(+)-ATPases: models for molecular structure-function studies. *Metallomics : integrated biometal science* **8**, 906-914
24. Singleton, C., and Le Brun, N. E. (2007) Atx1-like chaperones and their cognate P-type ATPases: copper-binding and transfer. *Biometals* **20**, 275-289
25. Ding, C., Festa, R. A., Chen, Y. L., Espart, A., Palacios, O., Espin, J., Capdevila, M., Atrian, S., Heitman, J., and Thiele, D. J. (2013) *Cryptococcus neoformans* copper detoxification machinery is critical for fungal virulence. *Cell Host Microbe* **13**, 265-276
26. Kay, K. L., Hamilton, C. J., and Le Brun, N. E. (2016) Mass spectrometry of *B. subtilis* CopZ: Cu(i)-binding and interactions with bacillithiol. *Metallomics : integrated biometal science* **8**, 709-719
27. Osterberg, R., Ligaarden, R., and Persson, D. (1979) Copper(I) complexes of penicillamine and glutathione. *Journal of inorganic biochemistry* **10**, 341-355
28. Rajkarnikar, A., Strankman, A., Duran, S., Vargas, D., Roberts, A. A., Barretto, K., Upton, H., Hamilton, C. J., and Rawat, M. (2013) Analysis of mutants disrupted in bacillithiol metabolism in *Staphylococcus aureus*. *Biochem Biophys Res Commun* **436**, 128-133
29. Helbig, K., Bleuel, C., Krauss, G. J., and Nies, D. H. (2008) Glutathione and transition-metal homeostasis in *Escherichia coli*. *J Bacteriol* **190**, 5431-5438
30. Grossoehme, N., Kehl-Fie, T. E., Ma, Z., Adams, K. W., Cowart, D. M., Scott, R. A., Skaar, E. P., and Giedroc, D. P. (2011) Control of copper resistance and inorganic sulfur metabolism by paralogous regulators in *Staphylococcus aureus*. *J Biol Chem* **286**, 13522-13531
31. Sitthisak, S., Knutsson, L., Webb, J. W., and Jayaswal, R. K. (2007) Molecular characterization of the copper transport system in *Staphylococcus aureus*. *Microbiology* **153**, 4274-4283
32. Radford, D. S., Kihlken, M. A., Borrelly, G. P., Harwood, C. R., Le Brun, N. E., and Cavet, J. S. (2003) CopZ from *Bacillus subtilis* interacts in vivo with a copper exporting CPx-type ATPase CopA. *FEMS Microbiol Lett* **220**, 105-112
33. Baker, J., Sengupta, M., Jayaswal, R. K., and Morrissey, J. A. (2011) The *Staphylococcus aureus* CsoR regulates both chromosomal and plasmid-encoded copper resistance mechanisms. *Environmental microbiology* **13**, 2495-2507
34. Zapotoczna, M., Riboldi, G. P., Moustafa, A. M., Dickson, E., Narechania, A., Morrissey, J. A., Planet, P. J., Holden, M. T. G., Waldron, K. J., and Geoghegan, J. A. (2018) Mobile-Genetic-Element-Encoded Hypertolerance to Copper Protects Staphylococcus aureus from Killing by Host Phagocytes. *mBio* **9**
35. Sitthisak, S., Howieson, K., Amezola, C., and Jayaswal, R. K. (2005) Characterization of a multicopper oxidase gene from *Staphylococcus aureus*. *Appl Environ Microbiol* **71**, 5650-5653

36. Arguello, J. M., Eren, E., and Gonzalez-Guerrero, M. (2007) The structure and function of heavy metal transport P1B-ATPases. *Biometals* **20**, 233-248
37. Odermatt, A., Suter, H., Krapf, R., and Solioz, M. (1993) Primary structure of two P-type ATPases involved in copper homeostasis in *Enterococcus hirae*. *J Biol Chem* **268**, 12775-12779
38. Marchler-Bauer, A., Derbyshire, M. K., Gonzales, N. R., Lu, S., Chitsaz, F., Geer, L. Y., Geer, R. C., He, J., Gwadz, M., Hurwitz, D. I., Lanczycki, C. J., Lu, F., Marchler, G. H., Song, J. S., Thanki, N., Wang, Z., Yamashita, R. A., Zhang, D., Zheng, C., and Bryant, S. H. (2015) CDD: NCBI's conserved domain database. *Nucleic Acids Res* **43**, D222-226
39. Li, M., Diep, B. A., Villaruz, A. E., Braughton, K. R., Jiang, X., DeLeo, F. R., Chambers, H. F., Lu, Y., and Otto, M. (2009) Evolution of virulence in epidemic community-associated methicillin-resistant *Staphylococcus aureus*. *Proc Natl Acad Sci U S A* **106**, 5883-5888
40. Perez-Perez, J. M., Candela, H., and Micol, J. L. (2009) Understanding synergy in genetic interactions. *Trends Genet* **25**, 368-376
41. Smaldone, G. T., and Helmann, J. D. (2007) CsoR regulates the copper efflux operon copZA in *Bacillus subtilis*. *Microbiology* **153**, 4123-4128
42. Bernsel, A., Viklund, H., Hennerdal, A., and Elofsson, A. (2009) TOPCONS: consensus prediction of membrane protein topology. *Nucleic Acids Res* **37**, W465-468
43. Hutchings, M. I., Palmer, T., Harrington, D. J., and Sutcliffe, I. C. (2009) Lipoprotein biogenesis in Gram-positive bacteria: knowing when to hold 'em, knowing when to fold 'em. *Trends Microbiol* **17**, 13-21
44. Rahman, O., Cummings, S. P., Harrington, D. J., and Sutcliffe, I. C. (2008) Methods for the bioinformatic identification of bacterial lipoproteins encoded in the genomes of Gram-positive bacteria. *World. J. Microbiol. Biotechnol.* **24**, 2377-2382
45. Navarre, W. W., Daefler, S., and Schneewind, O. (1996) Cell wall sorting of lipoproteins in *Staphylococcus aureus*. *J Bacteriol* **178**, 441-446
46. Kiedrowski, M. R., Crosby, H. A., Hernandez, F. J., Malone, C. L., McNamara, J. O., 2nd, and Horswill, A. R. (2014) *Staphylococcus aureus* Nuc2 is a functional, surface-attached extracellular nuclease. *PLoS One* **9**, e95574
47. Xiao, Z., Loughlin, F., George, G. N., Howlett, G. J., and Wedd, A. G. (2004) C-terminal domain of the membrane copper transporter Ctr1 from *Saccharomyces cerevisiae* binds four Cu(I) ions as a cuprous-thiolate polynuclear cluster: sub-femtomolar Cu(I) affinity of three proteins involved in copper trafficking. *J Am Chem Soc* **126**, 3081-3090
48. Xiao, Z., Gottschlich, L., van der Meulen, R., Udagedara, S. R., and Wedd, A. G. (2013) Evaluation of quantitative probes for weaker Cu(i) binding sites completes a set of four capable of detecting Cu(i) affinities from nanomolar to attomolar. *Metallomics : integrated biometal science* **5**, 501-513
49. Montelione, G. T. (2012) The Protein Structure Initiative: achievements and visions for the future. *F1000 Biol Rep* **4**, 7
50. Bertini, I., Cavallaro, G., and McGreevy, K. S. (2010) Cellular copper management-a draft user's guide. *Coord. Chem. Rev.* **254**, 506-524
51. Rubino, J. T., and Franz, K. J. (2012) Coordination chemistry of copper proteins: how nature handles a toxic cargo for essential function. *Journal of inorganic biochemistry* **107**, 129-143
52. Holm, L., and Laakso, L. M. (2016) Dali server update. *Nucleic Acids Res* **44**, W351-355
53. Ma, Z., Cowart, D. M., Ward, B. P., Arnold, R. J., DiMarchi, R. D., Zhang, L., George, G. N., Scott, R. A., and Giedroc, D. P. (2009) Unnatural amino acid

substitution as a probe of the allosteric coupling pathway in a mycobacterial Cu(I) sensor. *J Am Chem Soc* **131**, 18044-18045
54. Purves, J., Thomas, J., Riboldi, G. P., Zapotoczna, M., Tarrant, E., Andrew, P. W., Londono, A., Planet, P. J., Geoghegan, J. A., Waldron, K. J., and Morrissey, J. A. (2018) A horizontally gene transferred copper resistance locus confers hyper-resistance to antibacterial copper toxicity and enables survival of community acquired methicillin resistant *Staphylococcus aureus* USA300 in macrophages. *Environmental microbiology* **20**, 1576-1589
55. Ma, Z., Cowart, D. M., Scott, R. A., and Giedroc, D. P. (2009) Molecular insights into the metal selectivity of the copper(I)-sensing repressor CsoR from *Bacillus subtilis*. *Biochemistry* **48**, 3325-3334
56. Badarau, A., and Dennison, C. (2011) Copper trafficking mechanism of CXXC-containing domains: insight from the pH-dependence of their Cu(I) affinities. *J Am Chem Soc* **133**, 2983-2988
57. Singleton, C., and Le Brun, N. E. (2009) The N-terminal soluble domains of Bacillus subtilis CopA exhibit a high affinity and capacity for Cu(I) ions. *Dalton Trans*, 688-696
58. Singleton, C., Hearnshaw, S., Zhou, L., Le Brun, N. E., and Hemmings, A. M. (2009) Mechanistic insights into Cu(I) cluster transfer between the chaperone CopZ and its cognate Cu(I)-transporting P-type ATPase, CopA. *Biochem J* **424**, 347-356
59. Delmar, J. A., Su, C. C., and Yu, E. W. (2013) Structural mechanisms of heavy-metal extrusion by the Cus efflux system. *Biometals* **26**, 593-607
60. Bagchi, P., Morgan, M. T., Bacsa, J., and Fahrni, C. J. (2013) Robust affinity standards for Cu(I) biochemistry. *J Am Chem Soc* **135**, 18549-18559
61. Jabs, A., Weiss, M. S., and Hilgenfeld, R. (1999) Non-proline cis peptide bonds in proteins. *J Mol Biol* **286**, 291-304
62. Brandts, J. F., Halvorson, H. R., and Brennan, M. (1975) Consideration of the Possibility that the slow step in protein denaturation reactions is due to cis-trans isomerism of proline residues. *Biochemistry* **14**, 4953-4963
63. Schmidpeter, P. A., and Schmid, F. X. (2015) Prolyl isomerization and its catalysis in protein folding and protein function. *J Mol Biol* **427**, 1609-1631
64. Scholz, C., Scherer, G., Mayr, L. M., Schindler, T., Fischer, G., and Schmid, F. X. (1998) Prolyl isomerases do not catalyze isomerization of non-prolyl peptide bonds. *Biol Chem* **379**, 361-365
65. Pal, D., and Chakrabarti, P. (1999) Cis peptide bonds in proteins: residues involved, their conformations, interactions and locations. *J Mol Biol* **294**, 271-288
66. Planet, P. J., LaRussa, S. J., Dana, A., Smith, H., Xu, A., Ryan, C., Uhlemann, A. C., Boundy, S., Goldberg, J., Narechania, A., Kulkarni, R., Ratner, A. J., Geoghegan, J. A., Kolokotronis, S. O., and Prince, A. (2013) Emergence of the epidemic methicillin-resistant *Staphylococcus aureus* strain USA300 coincides with horizontal transfer of the arginine catabolic mobile element and speG-mediated adaptations for survival on skin. *mBio* **4**, e00889-00813
67. Zhang, Y. Q., Ren, S. X., Li, H. L., Wang, Y. X., Fu, G., Yang, J., Qin, Z. Q., Miao, Y. G., Wang, W. Y., Chen, R. S., Shen, Y., Chen, Z., Yuan, Z. H., Zhao, G. P., Qu, D., Danchin, A., and Wen, Y. M. (2003) Genome-based analysis of virulence genes in a non-biofilm-forming *Staphylococcus epidermidis* strain (ATCC 12228). *Mol Microbiol* **49**, 1577-1593
68. Lowder, B. V., Guinane, C. M., Ben Zakour, N. L., Weinert, L. A., Conway-Morris, A., Cartwright, R. A., Simpson, A. J., Rambaut, A., Nubel, U., and Fitzgerald, J. R. (2009) Recent human-to-poultry host jump, adaptation, and pandemic spread of *Staphylococcus aureus*. *Proc Natl Acad Sci U S A* **106**, 19545-19550

69. Resch, G., Francois, P., Morisset, D., Stojanov, M., Bonetti, E. J., Schrenzel, J., Sakwinska, O., and Moreillon, P. (2013) Human-to-bovine jump of *Staphylococcus aureus* CC8 is associated with the loss of a beta-hemolysin converting prophage and the acquisition of a new staphylococcal cassette chromosome. *PLoS One* **8**, e58187
70. Planet, P. J., Diaz, L., Kolokotronis, S. O., Narechania, A., Reyes, J., Xing, G., Rincon, S., Smith, H., Panesso, D., Ryan, C., Smith, D. P., Guzman, M., Zurita, J., Sebra, R., Deikus, G., Nolan, R. L., Tenover, F. C., Weinstock, G. M., Robinson, D. A., and Arias, C. A. (2015) Parallel Epidemics of Community-Associated Methicillin-Resistant *Staphylococcus aureus* USA300 Infection in North and South America. *J Infect Dis* **212**, 1874-1882
71. Hao, X., Luthje, F. L., Qin, Y., McDevitt, S. F., Lutay, N., Hobman, J. L., Asiani, K., Soncini, F. C., German, N., Zhang, S., Zhu, Y. G., and Rensing, C. (2015) Survival in amoeba--a major selection pressure on the presence of bacterial copper and zinc resistance determinants? Identification of a "copper pathogenicity island". *Appl Microbiol Biotechnol* **99**, 5817-5824
72. Pang, Y. Y., Schwartz, J., Bloomberg, S., Boyd, J. M., Horswill, A. R., and Nauseef, W. M. (2013) Methionine Sulfoxide Reductases Protect against Oxidative Stress in *Staphylococcus aureus* Encountering Exogenous Oxidants and Human Neutrophils. *J Innate Immun*
73. Mashruwala, A. A., Bhatt, S., Poudel, S., Boyd, E. S., and Boyd, J. M. (2016) The DUF59 Containing Protein SufT Is Involved in the Maturation of Iron-Sulfur (FeS) Proteins during Conditions of High FeS Cofactor Demand in *Staphylococcus aureus*. *PLoS Genet* **12**, e1006233
74. Kreiswirth, B. N., Lofdahl, S., Betley, M. J., O'Reilly, M., Schlievert, P. M., Bergdoll, M. S., and Novick, R. P. (1983) The toxic shock syndrome exotoxin structural gene is not detectably transmitted by a prophage. *Nature* **305**, 709-712
75. Novick, R. P. (1991) Genetic systems in staphylococci. *Methods Enzymol* **204**, 587-636
76. Rosario-Cruz, Z., Chahal, H. K., Mike, L. A., Skaar, E. P., and Boyd, J. M. (2015) Bacillithiol has a role in Fe-S cluster biogenesis in *Staphylococcus aureus*. *Mol Microbiol* **98**, 218-242
77. Bose, J. L., Fey, P. D., and Bayles, K. W. (2013) Genetic tools to enhance the study of gene function and regulation in *Staphylococcus aureus*. *Appl Environ Microbiol* **79**, 2218-2224
78. Mashruwala, A. A., Guchte, A. V., and Boyd, J. M. (2017) Impaired respiration elicits SrrAB-dependent programmed cell lysis and biofilm formation in *Staphylococcus aureus*. *Elife* **6**
79. Forsyth, R. A., Haselbeck, R. J., Ohlsen, K. L., Yamamoto, R. T., Xu, H., Trawick, J. D., Wall, D., Wang, L., Brown-Driver, V., Froelich, J. M., C, K. G., King, P., McCarthy, M., Malone, C., Misiner, B., Robbins, D., Tan, Z., Zhu Zy, Z. Y., Carr, G., Mosca, D. A., Zamudio, C., Foulkes, J. G., and Zyskind, J. W. (2002) A genome-wide strategy for the identification of essential genes in *Staphylococcus aureus*. *Mol Microbiol* **43**, 1387-1400
80. Mashruwala, A. A., Pang, Y. Y., Rosario-Cruz, Z., Chahal, H. K., Benson, M. A., Mike, L. A., Skaar, E. P., Torres, V. J., Nauseef, W. M., and Boyd, J. M. (2015) Nfu facilitates the maturation of iron-sulfur proteins and participates in virulence in *Staphylococcus aureus*. *Mol Microbiol* **95**, 383-409
81. Malone, C. L., Boles, B. R., Lauderdale, K. J., Thoendel, M., Kavanaugh, J. S., and Horswill, A. R. (2009) Fluorescent reporters for *Staphylococcus aureus*. *J Microbiol Methods* **77**, 251-260

82. Joska, T. M., Mashruwala, A., Boyd, J. M., and Belden, W. J. (2014) A universal cloning method based on yeast homologous recombination that is simple, efficient, and versatile. *J Microbiol Methods* **100**, 46-51
83. Mashruwala, A. A., and Boyd, J. M. (2015) De Novo Assembly of Plasmids Using Yeast Recombinational Cloning. *Methods Mol Biol* **1373**, 33-41
84. Roberts, C. A., Al-Tameemi, H. M., Mashruwala, A. A., Rosario-Cruz, Z., Chauhan, U., Sause, W. E., Torres, V. J., Belden, W. J., and Boyd, J. M. (2017) The Suf iron-sulfur cluster biosynthetic system is essential in *Staphylococcus aureus* and decreased Suf function results in global metabolic defects and reduced survival in human neutrophils. *Infect Immun*
85. Ranjit, D. K., Endres, J. L., and Bayles, K. W. (2011) *Staphylococcus aureus* CidA and LrgA proteins exhibit holin-like properties. *J Bacteriol* **193**, 2468-2476
86. Olson, B. J., and Markwell, J. (2007) Assays for determination of protein concentration. *Current protocols in protein science / editorial board, John E. Coligan ... [et al.]* **Chapter 3**, Unit 3 4
87. Xiao, R., Anderson, S., Aramini, J., Belote, R., Buchwald, W. A., Ciccosanti, C., Conover, K., Everett, J. K., Hamilton, K., Huang, Y. J., Janjua, H., Jiang, M., Kornhaber, G. J., Lee, D. Y., Locke, J. Y., Ma, L. C., Maglaqui, M., Mao, L., Mitra, S., Patel, D., Rossi, P., Sahdev, S., Sharma, S., Shastry, R., Swapna, G. V., Tong, S. N., Wang, D., Wang, H., Zhao, L., Montelione, G. T., and Acton, T. B. (2010) The high-throughput protein sample production platform of the Northeast Structural Genomics Consortium. *J Struct Biol* **172**, 21-33
88. Jansson, M., Li, Y. C., Jendeberg, L., Anderson, S., Montelione, G. T., and Nilsson, B. (1996) High-level production of uniformly (1)(5)N- and (1)(3)C-enriched fusion proteins in *Escherichia coli*. *J Biomol NMR* **7**, 131-141
89. Acton, T. B., Xiao, R., Anderson, S., Aramini, J., Buchwald, W. A., Ciccosanti, C., Conover, K., Everett, J., Hamilton, K., Huang, Y. J., Janjua, H., Kornhaber, G., Lau, J., Lee, D. Y., Liu, G., Maglaqui, M., Ma, L., Mao, L., Patel, D., Rossi, P., Sahdev, S., Shastry, R., Swapna, G. V., Tang, Y., Tong, S., Wang, D., Wang, H., Zhao, L., and Montelione, G. T. (2011) Preparation of protein samples for NMR structure, function, and small-molecule screening studies. *Methods Enzymol* **493**, 21-60
90. Kay, L. E., Torchia, D. A., and Bax, A. (1989) Backbone dynamics of proteins as studied by 15N inverse detected heteronuclear NMR spectroscopy: application to staphylococcal nuclease. *Biochemistry* **28**, 8972-8979
91. Delaglio, F., Grzesiek, S., Vuister, G. W., Zhu, G., Pfeifer, J., and Bax, A. (1995) NMRPipe: a multidimensional spectral processing system based on UNIX pipes. *J Biomol NMR* **6**, 277-293
92. Güntert, P., Dötsch, V., Wider, G., and Wüthrich, K. (1992) Processing of multi-dimensional NMR data with the new software PROSA. *J. Biomol. NMR.* **2**, 619-629
93. Keller, R. L. J. (2004) *The computer aided resonance assignment tutorial.*, CANTINA Verlag, Switzerland
94. Bartels, C., Xia, T. H., Billeter, M., Guntert, P., and Wuthrich, K. (1995) The program XEASY for computer-supported NMR spectral analysis of biological macromolecules. *J Biomol NMR* **6**, 1-10
95. Goddard, T. D., and Knelle, D. G. SPARKY 3. University of California, San Francisco
96. Harris, R. K., Becker, E. D., Cabral de Menezes, S. M., Granger, P., Hoffman, R. E., and Zilm, K. W. (2008) Further conventions for NMR shielding and chemical shifts (IUPAC Recommendations 2008). *Pure Appl. Chem.* **80**, 59-84
97. Bahrami, A., Assadi, A. H., Markley, J. L., and Eghbalnia, H. R. (2009) Probabilistic interaction network of evidence algorithm and its application to complete labeling of peak lists from protein NMR spectroscopy. *PLoS Comput Biol* **5**, e1000307

98. Neri, D., Szyperski, T., Otting, G., Senn, H., and Wuthrich, K. (1989) Stereospecific nuclear magnetic resonance assignments of the methyl groups of valine and leucine in the DNA-binding domain of the 434 repressor by biosynthetically directed fractional 13C labeling. *Biochemistry* **28**, 7510-7516
99. Pelton, J. G., Torchia, D. A., Meadow, N. D., and Roseman, S. (1993) Tautomeric states of the active-site histidines of phosphorylated and unphosphorylated IIIGlc, a signal-transducing protein from *Escherichia coli*, using two-dimensional heteronuclear NMR techniques. *Protein Sci* **2**, 543-558
100. Ulrich, E. L., Akutsu, H., Doreleijers, J. F., Harano, Y., Ioannidis, Y. E., Lin, J., Livny, M., Mading, S., Maziuk, D., Miller, Z., Nakatani, E., Schulte, C. F., Tolmie, D. E., Kent Wenger, R., Yao, H., and Markley, J. L. (2008) BioMagResBank. *Nucleic Acids Res* **36**, D402-408
101. Shen, Y., Delaglio, F., Cornilescu, G., and Bax, A. (2009) TALOS+: a hybrid method for predicting protein backbone torsion angles from NMR chemical shifts. *J Biomol NMR* **44**, 213-223
102. Huang, Y. J., Tejero, R., Powers, R., and Montelione, G. T. (2006) A topology-constrained distance network algorithm for protein structure determination from NOESY data. *Proteins* **62**, 587-603
103. Guntert, P., Mumenthaler, C., and Wuthrich, K. (1997) Torsion angle dynamics for NMR structure calculation with the new program DYANA. *J Mol Biol* **273**, 283-298
104. Tjandra, N., Grzesiek, S., and Bax, A. (1996) Magnetic field dependence of nitrogen−proton J splittings in 15N-enriched human ubiquitin resulting from relaxation interference and residual dipolar coupling. *J Am Chem Soc* **118**, 6264-6272
105. Linge, J. P., Williams, M. A., Spronk, C. A., Bonvin, A. M., and Nilges, M. (2003) Refinement of protein structures in explicit solvent. *Proteins* **50**, 496-506
106. Brunger, A. T., Adams, P. D., Clore, G. M., DeLano, W. L., Gros, P., Grosse-Kunstleve, R. W., Jiang, J. S., Kuszewski, J., Nilges, M., Pannu, N. S., Read, R. J., Rice, L. M., Simonson, T., and Warren, G. L. (1998) Crystallography & NMR system: A new software suite for macromolecular structure determination. *Acta Crystallogr D Biol Crystallogr* **54**, 905-921
107. Bhattacharya, A., Tejero, R., and Montelione, G. T. (2007) Evaluating protein structures determined by structural genomics consortia. *Proteins* **66**, 778-795
108. Huang, Y. J., Powers, R., and Montelione, G. T. (2005) Protein NMR recall, precision, and F-measure scores (RPF scores): structure quality assessment measures based on information retrieval statistics. *J Am Chem Soc* **127**, 1665-1674
109. Koradi, R., Billeter, M., and Wuthrich, K. (1996) MOLMOL: a program for display and analysis of macromolecular structures. *J Mol Graph* **14**, 51-55, 29-32
110. Schrödinger, L. The PyMOL Molecular Graphics System, Version 1.8
111. Ashkenazy, H., Erez, E., Martz, E., Pupko, T., and Ben-Tal, N. (2010) ConSurf 2010: calculating evolutionary conservation in sequence and structure of proteins and nucleic acids. *Nucleic Acids Res* **38**, W529-533
112. Farmer, B. T., 2nd, Constantine, K. L., Goldfarb, V., Friedrichs, M. S., Wittekind, M., Yanchunas, J., Jr., Robertson, J. G., and Mueller, L. (1996) Localizing the NADP+ binding site on the MurB enzyme by NMR. *Nat Struct Biol* **3**, 995-997
113. Fey, P. D., Endres, J. L., Yajjala, V. K., Widhelm, T. J., Boissy, R. J., Bose, J. L., and Bayles, K. W. (2013) A genetic resource for rapid and comprehensive phenotype screening of nonessential *Staphylococcus aureus* genes. *mBio* **4**, e00537-00512

**Table 1. Strains and plasmids used in this study.**

***Staphylococcus aureus* strains**

| Strain name | Genotype/Description | Background | Source / Reference |
|---|---|---|---|
| RN4220 | Restriction-negative | RN1 | (74) |
| JMB2790 | *copA*::Tn(*ermB*) (SAUSA300_2494) | JE2 | (113) |
| JMB3488 | *csoR*::Tn(*ermB*) (SAUSA300_2043) | JE2 | (113) |
| JMB1100 | USA300 wild-type strain | LAC | A.R. Horswill |
| JMB4084 | *copA*::Tn(*ermB*) | LAC | This study |
| JMB6807 | *csoR*::Tn(*tet*) | LAC | This study |
| JMB7900 | Δ*copB* (SAUSA300_0078) | LAC | This study |
| JMB7711 | Δ*copL* (SAUSA300_0079) | LAC | This study |
| JMB7901 | Δ*copBL* | LAC | This study |
| JMB8009 | Δ*copB*, *copA*::Tn(*ermB*) | LAC | This study |
| JMB7803 | Δ*copL*, *copA*::Tn(*ermB*) | LAC | This study |
| JMB7972 | Δ*copBL*, *copA*::Tn(*ermB*) | LAC | This study |
| JMB1324 | parent strain | MW2 | P. Schlievert |
| JMB1325 | parent strain | COL | A. Horswill |
| JMB1422 | parent strain | Newman | E. Skaar |
| JMB6338 | Δ*csoR* (NWMN_1991) | Newman | (30) |

**Other Strains**

| Name | Relevant genotype/Description | Source / Reference |
|---|---|---|
| *Escherichia coli* DH5α | Molecular cloning | Protein Express |
| *E. coli* BL21 DE3 | Protein expression and purification | New England Biolabs |
| JMB7761 | *Bacillus subtilis* 168 (parent) | V. Carabetta |
| JMB7762 | *Bacillus subtilis* 168 Δ*ydhK*::ery (BSU05790) | V. Carabetta |
| *Saccharomyces cerevisiae* FY2 | *ura3-52* yeast recombination cloning | W. Belden |

**Plasmids**

| Plasmid name | Locus/Function | Source / Reference |
|---|---|---|
| pJB38 | Mutant construction | (77) |
| pTET | pJB38 with *tetM* | (77) |
| pJB38_Δ*copB* | Δ*copB* chromosomal deletion | This study |
| pJB38_Δ*copL* | Δ*copL* chromosomal deletion | This study |
| pJB38_Δ*copBL* | Δ*copBL* chromosomal deletion | This study |
| pCM11 | Promoterless *gfp* for transcriptional studies | (81) |
| pEPSA5 | Genetic complementation; XylRO promoter | (79) |
| pCM11_*copB* | *copB* transcriptional reporter | This study |
| pEPSA5_*copB* | *copB* complementation | This study |
| pEPSA5_*copL* | *copL* complementation | This study |
| pEPSA5_*copL*(T) | truncated *copL* complementation | This study |
| pEPSA5_*copL*-FLAG | *copL* containing a C-terminal FLAG tag | This study |
| pEPSA5_*nuc2*(FL)-*copL* | *nuc2* fused to *copL* | This study |
| pEPSA5_*copL*(T)-FLAG | truncated *copL* containing a C-terminal FLAG tag | This study |
| pEPSA5_*nuc2*(SS)-*copL* | *nuc2* signal sequence fused to truncated *copL* | This study |
| pEPSA5_*nuc2*(SS)-*copL** | *nuc2* signal sequence fused to truncated *copL** | This study |
| pGEX-6P-1 | gene expression for protein purification | GE Healthcare |
| pGEX-6P-1_*copL* | CopL expression | This study |
| pGEX-6P-1_*copL** | CopL* expression | This study |

## FIGURE LEGENDS.

**Figure 1. CopB and CopL protect against Cu toxicity in *S. aureus*.**
(A) Chromosomal location of genes involved in Cu homeostasis in *S. aureus* USA300_FPR3757. The *copB* and *copL* genes are located in the Arginine Catabolic Mobile Element (ACME), adjacent to the SCC*mec*IV genetic element. Locus tags are provided below the genes. (B) The *copA*, *copB*, and *copL* gene products are required to protect against Cu toxicity. Top: The WT (JMB1100) and Δ*copB* (JMB7900) strains containing pEPSA5 or pEPSA5_*copB* are shown. Bottom: The WT and Δ*copL* (JMB7711) strains containing pEPSA5 or pEPSA5_*copL* are shown. Strains were serial diluted and spot plated on chemically defined media with or without 50 μM Cu. (C) Overexpression of *copB* or *copL* results in increased Cu resistance in the *S. aureus* USA400 strain MW2. The *S. aureus* USA400 clone MW2, which lacks genome encoded *copB* and *copL*, containing pEPSA5, pEPSA5_*copB*, or pEPSA_*copL* is shown. Strains were serial diluted and spot plated on chemically defined media without or with 100 μM Cu.

**Figure 2. Intracellular Cu accumulation exacerbates the phenotypes of the *copB* and *copL* mutants and CopA, CopB, and CopL function independently.**
(A) The phenotypes associated with *copA* and *copB* mutations are synergistic. The WT (JMB1100), *copA::Tn* (JMB4084), Δ*copB* (JMB7900), and *copA::Tn* Δ*copB* (JMB8009) strains were serial diluted and spot plated on chemically defined media without or with 50 μM Cu. (B) The phenotypes associated with *copB* and *copL* mutations are additive. The WT, Δ*copL* (JMB7711), *copA::Tn*, and *copA::Tn* Δ*copL* (JMB7803) strains were serial diluted and spot plated on chemically defined media without or with 50 μM Cu. (C) CopA, CopB, and CopL function independently to protect against Cu toxicity. The WT, *copA::Tn* Δ*copB*, *copA::Tn* Δ*copL*, Δ*copB* Δ*copL* (JMB7901), and *copA::Tn* Δ*copB* Δ*copL* (JMB7972) strains were serial diluted and spot plated on chemically defined media without or with 10 μM Cu.

**Figure 3. The *copBL* operon is upregulated under copper stress.**
(A) The *copA*, *copB*, and *copL* genes are induced by Cu. The *S. aureus* WT (JMB1100) was cultured in chemically defined media containing 0 μM or 100 μM Cu. RNA was isolated, cDNA generated, and the abundance of the *copA*, *copB*, and *copL* transcripts were quantified using qPCR. Data show fold-induction of genes of interest upon addition of Cu with respect to no Cu addition. Data represent the average of biological triplicates with errors presented as standard deviations. (B) The *copB* and *copL* genes are co-transcribed. RNA was isolated from the WT grown in chemically defined medium with 100 μM Cu and cDNA libraries generated. (i) Schematic showing the primer pair (ZRT21 and ZRT24) used to detect the *copBL* transcript; expected size: 643 base pairs. (ii) Agarose gel electrophoresis was used to detect the *copBL* amplicon generated using cDNA libraries as template DNA. A reaction without reverse transcriptase (-RT) was included as a control for genomic DNA contamination. (C) Transcriptional activity of *copB* increases in synchrony with Cu concentration. Transcriptional activity of the *copB* reporter was monitored in the *S. aureus* USA300 WT grown in chemically defined media containing 0, 50, 100, or 200 μM Cu. (D) Transcriptional activity of *copB* is specific to copper stress. Transcriptional activity of *copB* was monitored in the WT grown in chemically defined media containing 100 μM $Cu^{2+}$, 100 μM $Mn^{2+}$, 100 μM $Fe^{2+}$, 100 μM $Zn^{2+}$, or 50 μM $Co^{2+}$. For Panels (C) and (D), fluorescence data was standardized to culture optical density ($A_{590}$) and data represent the average of biological triplicates with errors presented as standard deviations. Students t-test were performed on the data and * indicates $P \leq 0.05$.

**Figure 4. Transcription of the *copBL* operon is regulated by CsoR.**
(A) The proposed CsoR binding sites are shown for the *S. aureus* USA300_FPR3757 *copA* and *copB* promoter regions, as well as the *B. subtilis copZ* and *S. aureus* Newman *copA* promoter regions. (B) Transcriptional activity of *copB* is increased in a *csoR* mutant. Transcriptional activity of *copB* was monitored in the WT (JMB1100) and *csoR::Tn* (JMB6807) strains grown in chemically defined media containing 0 μM or 100 μM Cu. Fluorescence data was standardized to culture optical density ($A_{590}$). Data shown represent the average of biological triplicates with errors presented as standard deviations.

Students t-test were performed on the data and * indicates P $\leq$ 0.05, whereas N.S. denotes not significant.

**Figure 5. CopL is membrane-associated and surface-exposed**.
(A) Monitoring CopL abundance in *S. aureus* whole cell extracts, cytosolic fractions, and membrane fractions. The Δ*copL* (JMB7711) mutant containing the pEPSA or pEPSA5_*copL*-FLAG were cultured in the absence and presence of 0.2% xylose prior to fractionation and analysis. ND; not detected. Representative densitometry and Western blot (inset) analysis shown. (B) The membrane-anchor signal-sequence is necessary for CopL function. (i) Schematic showing the CopL variants utilized. The pEPSA_*copL* encoded saCopL and pEPSA_*copL*(T) encoded for the truncated saCopL(T), which lacked the proposed N-terminus export signal-sequence and lipobox. (ii) The WT and Δ*copL* strains harboring the pEPSA5, pEPSA5_*copL*, or pEPSA5_*copL*(T) were serial diluted and spot plated on chemically defined media without and with 100 μM Cu. (C) Cell surface exposure is necessary for CopL function. (i) Schematic showing the CopL-Nuc2 chimeric variants. The truncated *copL* gene, lacking the proposed N-terminal export-sequence and lipobox, was fused to either the full length *nuc2* or the *nuc2* membrane-anchor signal-sequence and cloned into the pEPSA5 plasmid to yield the pEPSA5_*nuc2*(FL)-*copL* and pEPSA5_*nuc2*(SS)-*copL* vectors, respectively. (ii) The WT and Δ*copL* strains harboring pEPSA5, pEPSA5_*nuc2*(FL)-*copL*, or pEPSA5_*nuc2*(SS)-*copL* were serial diluted and spot plated on chemically defined media containing 0 μM or 100 μM Cu.

**Figure 6. The *S. aureus* CopL (saCopL) binds $Cu^{1+}$ *in vitro*.**
(A) saCopL binds approximately 4 molar equivalents of $Cu^{1+}$. Apo-CopL (12.5 μM) was anaerobically titrated with $Cu^{1+}$ and binding was monitored by measuring absorbance at 243 nm using UV absorption spectroscopy. (B) the affinity of saCopL for $Cu^{1+}$ was monitored by BCS displacement. Solutions containing 0.5 mM BCS and 20 μM $Cu^{1+}$ were titrated with apo-saCopL(T) and BCS displacement was monitored by measuring absorbance at 483 nm using visible absorption spectroscopy.

**Figure 7. Solution NMR structure of *B. subtilis* CopL.**
(A) Ribbon diagram of the lowest-energy conformer of *B. subtilis* CopL: backbone of β-strands shown in cyan, short $3_{10}$-helical segments in red/yellow, other polypeptide segments in gray; the terminal Lys83 and Lys205 are labeled as "N" and "C". Side chains of Lys131-Trp132 and Lys195-Trp196 residue pairs connected by unusual *cis*-peptide bonds are shown in blue. Moieties presumed to be involved in coordinating Cu, side-chains of His94, Met95, Met98, His130, His158, Met159, Met162 and His194, as well as carbonyls of Lys131 and Lys195, are shown in red. (B) Space-filling representation of the same conformer showing the degree of residue conservation calculated with ConSurf. Conservation scores are arranged into nine groups with the corresponding colors ranging from cyan (most variable) to burgundy (most conserved). The numbering shown here is that of the UniProt entry BSU05790.

**Figure 8. Chemical shift perturbations of *B. subtilis* CopL due to $Cu^{1+}$ binding.**
Overlay of 600 MHz [$^{15}$N,$^{1}$H]-HSQC spectra of 0.3 mM apo-bsCopL-N (blue) and 0.3 mM holo-bsCopL-N with 6 mol/mol equivalents of $Cu^{1+}$ (red). The sequence-specific [$^{15}$N,$^{1}$H]-HSQC resonance assignments for apo-bsCopL-N are shown in Supplementary Figure S15.

**Figure 9. $Cu^{1+}$ binding to *B. subtilis* CopL.**
(A-C). Surface molecular representation of *B. subtilis* CopL, in three orientations, showing the locations of conserved residues His94, Met95, Met98 (buried), His129, His130, Lys131, His158, Met159, Met162 (buried), His194, and Lys195, presumed to be involved in coordinating $Cu^{1+}$. Only residues that can be seen on the surface of the 3D structure are labeled. (D-F) Surface representation of *B. subtilis* CopL, in same three orientations, showing chemical shift perturbations due to $Cu^{1+}$-binding. Color code: dark blue, ($\Delta\delta_{NH} > 0.25$ ppm, *viz.,* Thr92, Met95, His130, His131, Met179, Val180, Asn193, His194, Lys195); Cyan, residues with $H^{N}$ resonances that are broadened due to $Cu^{1+}$ -binding (*viz*, Trp132, Tyr178, Trp196, Val197, and Thr198); light grey, residues with $H^{N}$ resonances which are absent in the [$^{15}$N,$^{1}$H]-HSQC spectrum of apo-CopL and not assigned (*viz* Lys 83, His94, Lys 96, Gly97, Lys160, Gly161, and Ser187), and white for proline residues which lack backbone amide protons (*viz*, Pro120 and Pro148). (G-I) Ribbon representation of *B. subtilis* CopL, in same three orientations, showing

conformational perturbations due to $Cu^{1+}$-binding using the same color code as in panels D-F. In panels G - I, only the residues with $H^N$ resonances that are affected by $Cu^{1+}$-binding are labeled. The numbering shown here is that of the UniProt entry BSU05790.

**Figure 10. Effective Cu binding is necessary for CopL to protect against Cu toxicity.** (A) The *copL** allele does not correct the Cu-sensitivity phenotype of a *S. aureus* Δ*copL* mutant. (i) Schematic of the *copL* and *copL** constructs utilized. (ii) The WT and Δ*copL* strains harboring pEPSA5, pEPSA5_*nuc2*(SS)-*copL*, or pEPSA5_*nuc2*(SS)-*copL** were serial diluted and spot plated on chemically defined media without and with 100 μM Cu. (B) The saCopL(T)* binds less $Cu^{1+}$ than saCopL(T). 12.5 μM apo-saCopL(T) or apo-saCopL(T)* were anaerobically titrated with $Cu^{1+}$. Binding was monitored by measuring absorbance at 243 nm using UV absorption spectroscopy. (C) saCopL(T)* has a lower affinity for $Cu^{1+}$ than saCopL(T). Solutions containing 0.5 mM BCS and 20 μM $Cu^{1+}$ were titrated with either apo-saCopL(T) or apo-saCopL(T)*. Copper binding to CopL was examined using BCS displacement by monitoring sample absorbance at 483 nm, which is the absorption maxima for the $Cu^{1+}$-BCS complex. The data for the saCopL(T) are also presented in Figure 6 and included here for comparison.

**Figure 11. Working model for copper homeostasis in *S. aureus.***
The CsoR transcriptional regulator binds intracellular copper, leading to derepression of the *copAZ* and *copBL* operons. CopA and CopB are transmembrane copper-exporters. CopZ is a chaperone protein that binds copper and acts as a cytosolic buffer. CopL is a membrane-bound, surface-exposed, copper-binding lipoprotein. CopL likely functions in preventing copper uptake by binding extracellular Cu to prevent it from entering or re-entering the cell after export by CopB or CopA.

**FIGURE and LEGENDS.**

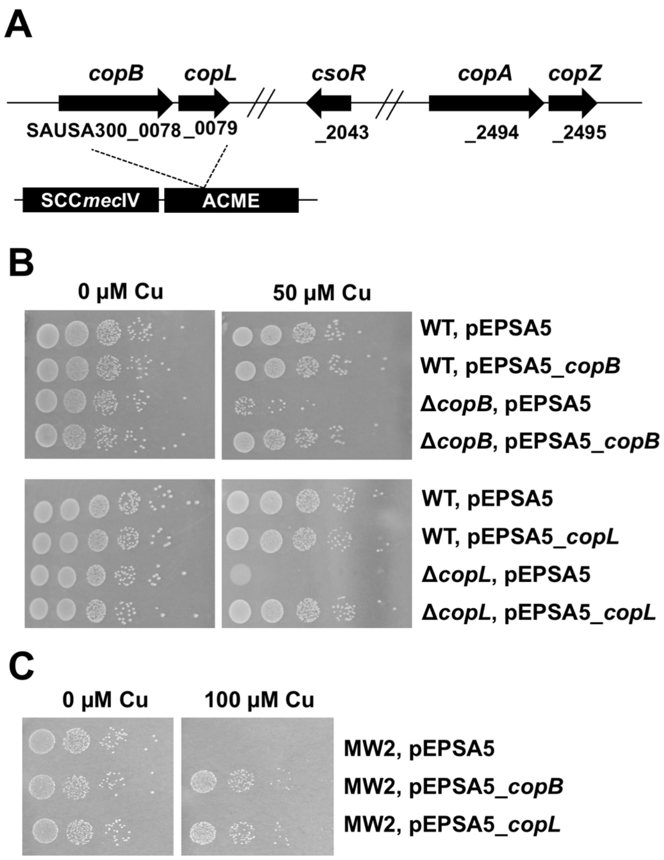


**Figure 1. CopB and CopL protect against Cu toxicity in *S. aureus*.**
(A) Chromosomal location of genes involved in Cu homeostasis in *S. aureus* USA300_FPR3757. The *copB* and *copL* genes are located in the Arginine Catabolic Mobile Element (ACME), adjacent to the SCC*mec*IV genetic element. Locus tags are provided below the genes. (B) The *copA*, *copB*, and *copL* gene products are required to protect against Cu toxicity. Top: The WT (JMB1100) and Δ*copB* (JMB7900) strains containing pEPSA5 or pEPSA5_*copB* are shown. Bottom: The WT and Δ*copL* (JMB7711) strains containing pEPSA5 or pEPSA5_*copL* are shown. Strains were serial diluted and spot plated on chemically defined media with or without 50 µM Cu. (C) Overexpression of *copB* or *copL* results in increased Cu resistance in the *S. aureus* USA400 strain MW2. The *S. aureus* USA400 clone MW2, which lacks genome encoded *copB* and *copL*, containing pEPSA5, pEPSA5_*copB*, or pEPSA_*copL* is shown. Strains were serial diluted and spot plated on chemically defined media without or with 100 µM Cu.

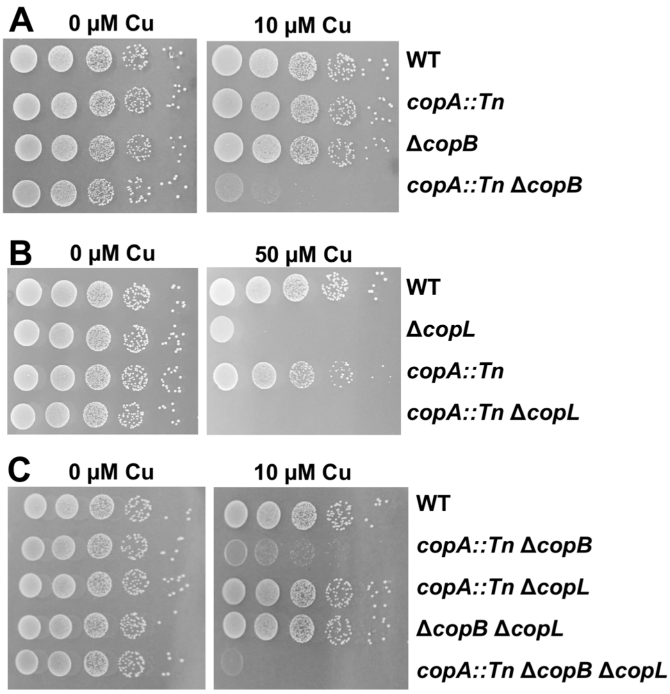


**Figure 2. Intracellular Cu accumulation exacerbates the phenotypes of the *copB* and *copL* mutants and CopA, CopB, and CopL function independently.**
(A) The phenotypes associated with *copA* and *copB* mutations are synergistic. The WT (JMB1100), *copA::Tn* (JMB4084), Δ*copB* (JMB7900), and *copA::Tn* Δ*copB* (JMB8009) strains were serial diluted and spot plated on chemically defined media without or with 50 µM Cu. (B) The phenotypes associated with *copB* and *copL* mutations are additive. The WT, Δ*copL* (JMB7711), *copA::Tn*, and *copA::Tn* Δ*copL* (JMB7803) strains were serial diluted and spot plated on chemically defined media without or with 50 µM Cu. (C) CopA, CopB, and CopL function independently to protect against Cu toxicity. The WT, *copA::Tn* Δ*copB*, *copA::Tn* Δ*copL*, Δ*copB* Δ*copL* (JMB7901), and *copA::Tn* Δ*copB* Δ*copL* (JMB7972) strains were serial diluted and spot plated on chemically defined media without or with 10 µM Cu.

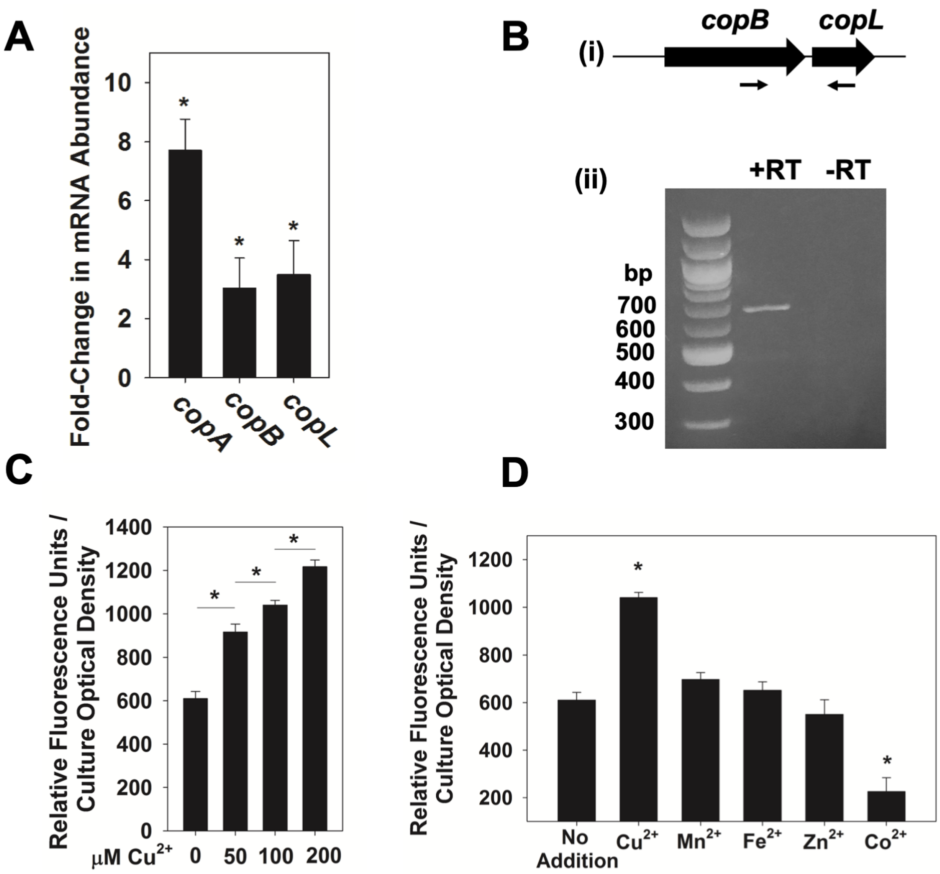


**Figure 3. The *copBL* operon is upregulated under copper stress.**
(A) The *copA*, *copB*, and *copL* genes are induced by Cu. The *S. aureus* WT (JMB1100) was cultured in chemically defined media containing 0 μM or 100 μM Cu. RNA was isolated, cDNA generated, and the abundance of the *copA*, *copB*, and *copL* transcripts were quantified using qPCR. Data show fold-induction of genes of interest upon addition of Cu with respect to no Cu addition. Data represent the average of biological triplicates with errors presented as standard deviations. (B) The *copB* and *copL* genes are co-transcribed. RNA was isolated from the WT grown in chemically defined medium with 100 μM Cu and cDNA libraries generated. (i) Schematic showing the primer pair (ZRT21 and ZRT24) used to detect the *copBL* transcript; expected size: 643 base pairs. (ii) Agarose gel electrophoresis was used to detect the *copBL* amplicon generated using cDNA libraries as template DNA. A reaction without reverse transcriptase (-RT) was included as a control for genomic DNA contamination. (C) Transcriptional activity of *copB* increases in synchrony with Cu concentration. Transcriptional activity of the *copB* reporter was monitored in the *S. aureus* USA300 WT grown in chemically defined media containing 0, 50, 100, or 200 μM Cu. (D) Transcriptional activity of *copB* is specific to copper stress. Transcriptional activity of *copB* was monitored in the WT grown in chemically defined media containing 100 μM $Cu^{2+}$, 100 μM $Mn^{2+}$, 100 μM $Fe^{2+}$, 100 μM $Zn^{2+}$, or 50 μM $Co^{2+}$. For Panels (C) and (D), fluorescence data was standardized to culture optical density ($A_{590}$) and data represent the average of biological triplicates with errors presented as standard deviations. Students t-test were performed on the data and * indicates $P \leq 0.05$.

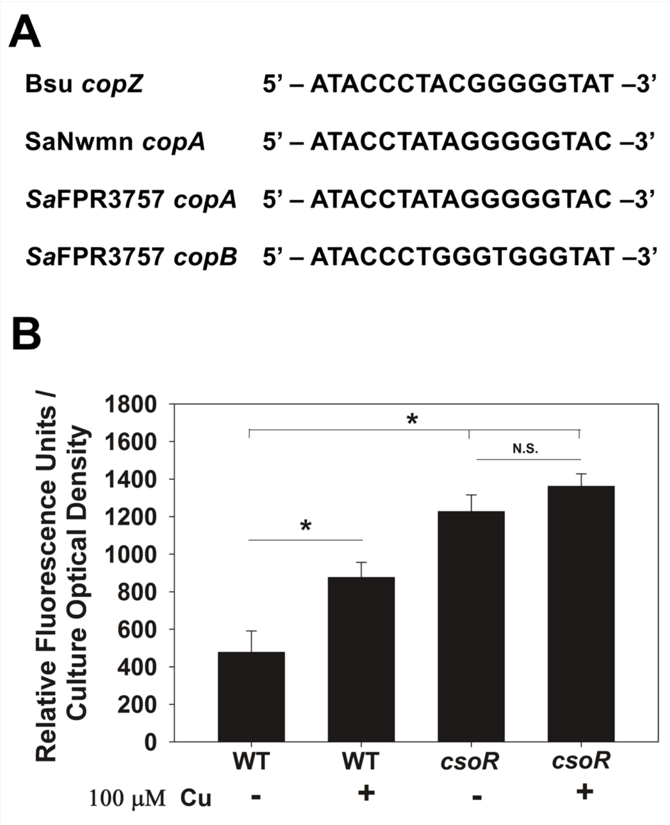


**Figure 4. Transcription of the *copBL* operon is regulated by CsoR.**
(A) The proposed CsoR binding sites are shown for the *S. aureus* USA300_FPR3757 *copA* and *copB* promoter regions, as well as the *B. subtilis copZ* and *S. aureus* Newman *copA* promoter regions. (B) Transcriptional activity of *copB* is increased in a *csoR* mutant. Transcriptional activity of *copB* was monitored in the WT (JMB1100) and *csoR::Tn* (JMB6807) strains grown in chemically defined media containing 0 μM or 100 μM Cu. Fluorescence data was standardized to culture optical density ($A_{590}$). Data shown represent the average of biological triplicates with errors presented as standard deviations. Students t-test were performed on the data and * indicates $P \leq 0.05$, whereas N.S. denotes not significant.

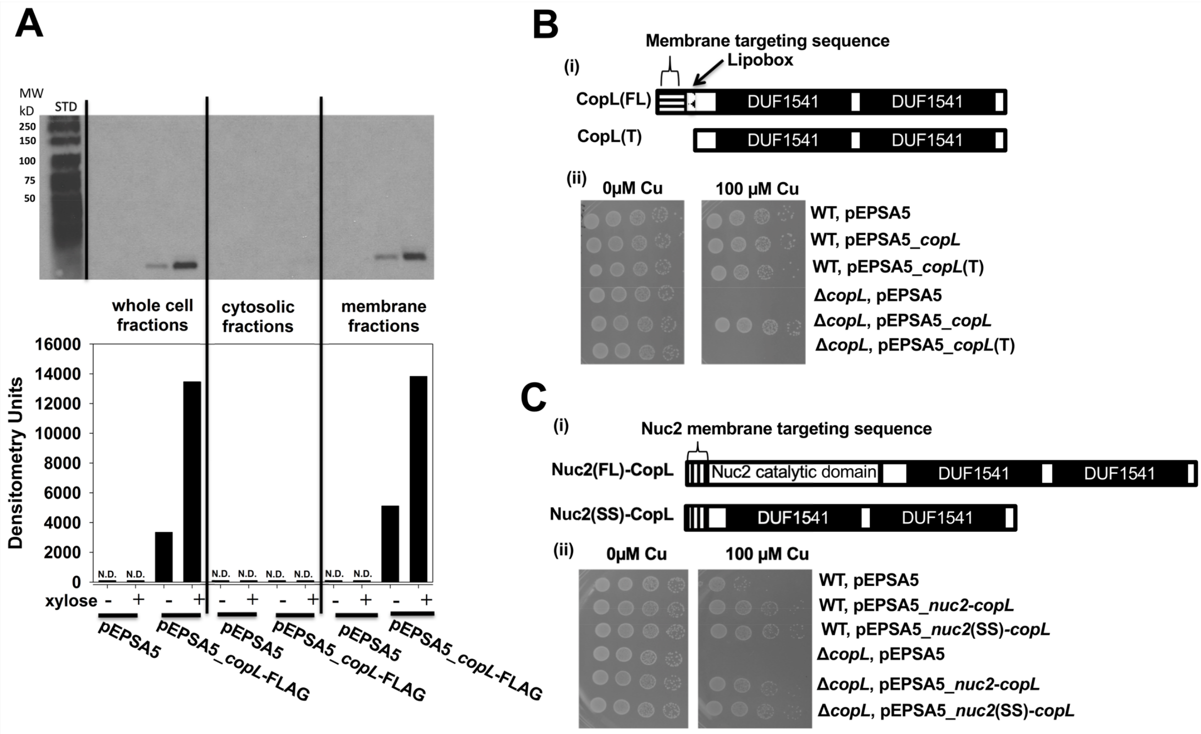


**Figure 5. CopL is membrane-associated and surface-exposed**.
(A) Monitoring CopL abundance in *S. aureus* whole cell extracts, cytosolic fractions, and membrane fractions. The Δ*copL* (JMB7711) mutant containing the pEPSA or pEPSA5_*copL*-FLAG were cultured in the absence and presence of 0.2% xylose prior to fractionation and analysis. ND; not detected. Representative densitometry and Western blot (inset) analysis shown. (B) The membrane-anchor signal-sequence is necessary for CopL function. (i) Schematic showing the CopL variants utilized. The pEPSA_*copL* encoded saCopL and pEPSA_*copL*(T) encoded for the truncated saCopL(T), which lacked the proposed N-terminus export signal-sequence and lipobox. (ii) The WT and Δ*copL* strains harboring the pEPSA5, pEPSA5_*copL*, or pEPSA5_*copL*(T) were serial diluted and spot plated on chemically defined media without and with 100 μM Cu. (C) Cell surface exposure is necessary for CopL function. (i) Schematic showing the CopL-Nuc2 chimeric variants. The truncated *copL* gene, lacking the proposed N-terminal export-sequence and lipobox, was fused to either the full length *nuc2* or the *nuc2* membrane-anchor signal-sequence and cloned into the pEPSA5 plasmid to yield the pEPSA5_*nuc2*(FL)-*copL* and pEPSA5_*nuc2*(SS)-*copL* vectors, respectively. (ii) The WT and Δ*copL* strains harboring pEPSA5, pEPSA5_*nuc2*(FL)-*copL*, or pEPSA5_*nuc2*(SS)-*copL* were serial diluted and spot plated on chemically defined media containing 0 μM or 100 μM Cu.

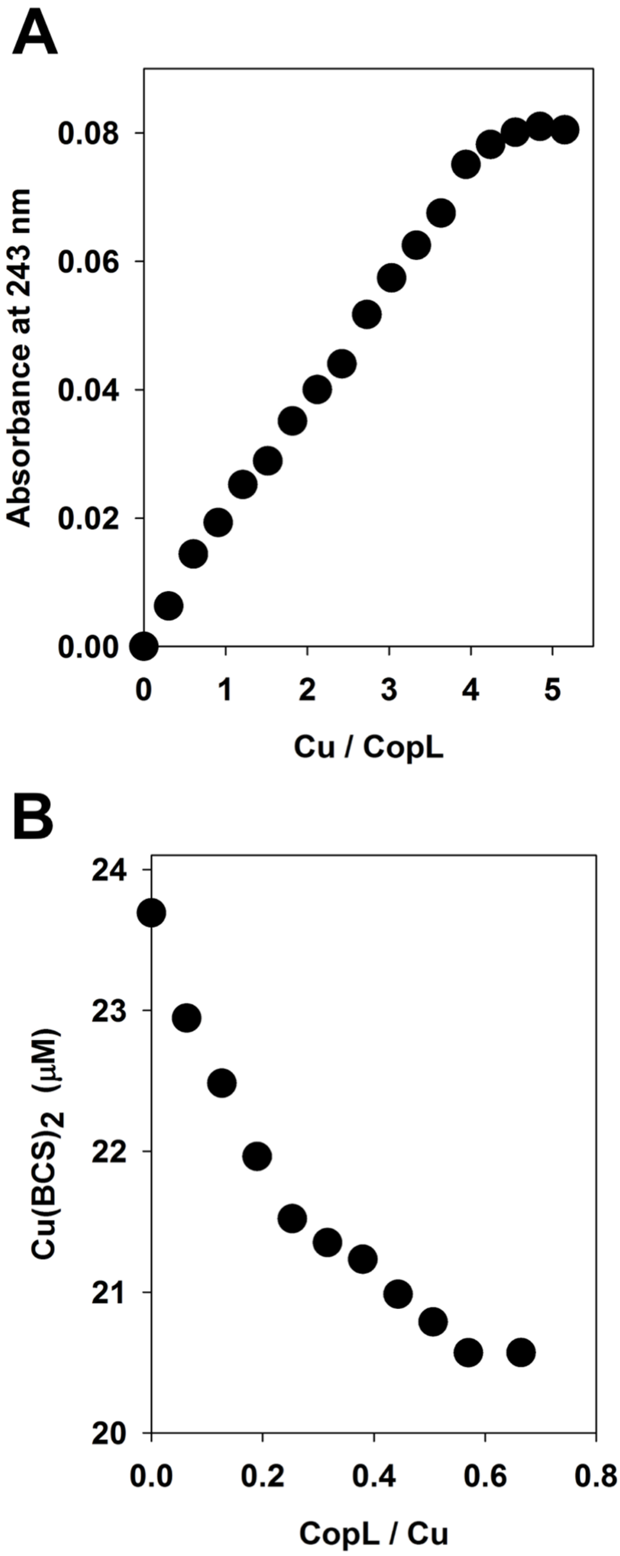


**Figure 6. The *S. aureus* CopL (saCopL) binds $Cu^{1+}$ *in vitro*.**
(A) saCopL binds approximately 4 molar equivalents of $Cu^{1+}$. Apo-CopL (12.5 µM) was anaerobically titrated with $Cu^{1+}$ and binding was monitored by measuring absorbance at 243 nm using UV absorption spectroscopy. (B) the affinity of saCopL for $Cu^{1+}$ was monitored by BCS displacement. Solutions containing 0.5 mM BCS and 20 µM $Cu^{1+}$ were titrated with apo-saCopL(T) and BCS displacement was monitored by measuring absorbance at 483 nm using visible absorption spectroscopy.

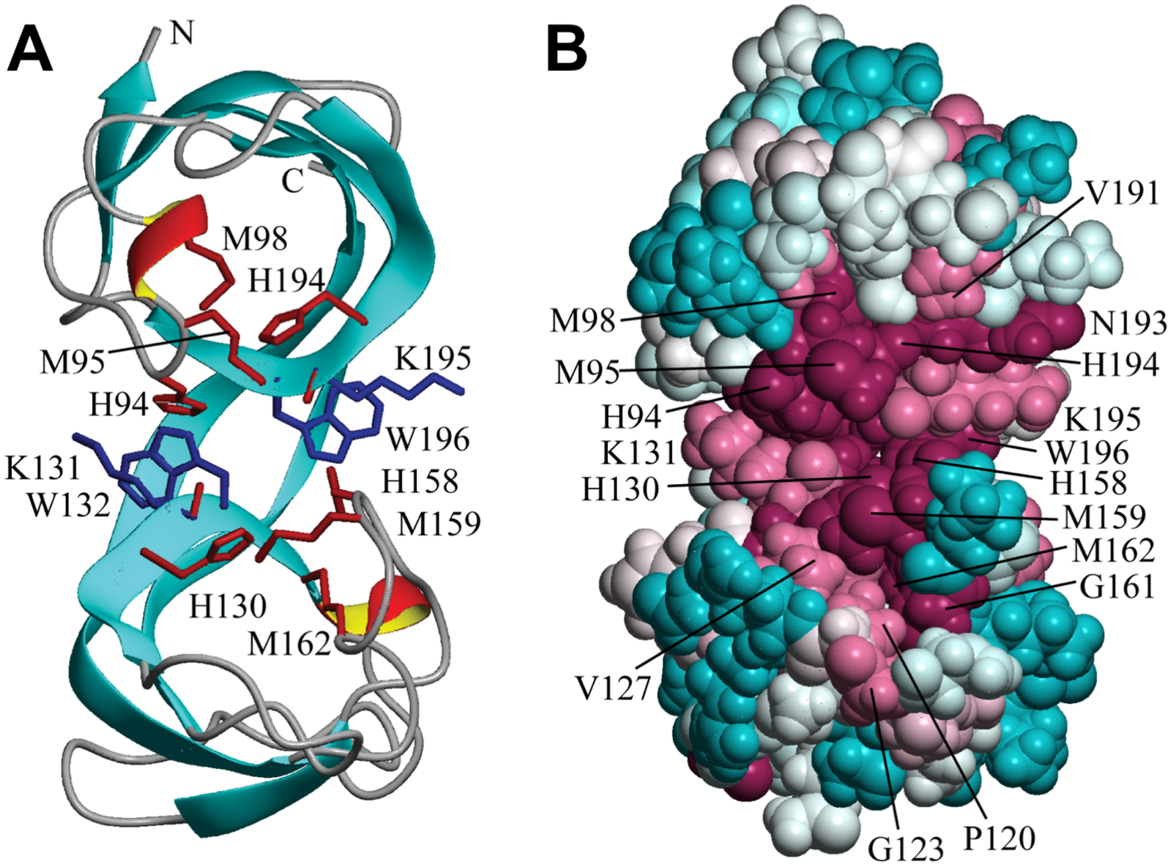


**Figure 7. Solution NMR structure of *B. subtilis* CopL.**
(A) Ribbon diagram of the lowest-energy conformer of *B. subtilis* CopL: backbone of β-strands shown in cyan, short $3_{10}$-helical segments in red/yellow, other polypeptide segments in gray; the terminal Lys83 and Lys205 are labeled as "N" and "C". Side chains of Lys131-Trp132 and Lys195-Trp196 residue pairs connected by unusual *cis*-peptide bonds are shown in blue. Moieties presumed to be involved in coordinating Cu, side-chains of His94, Met95, Met98, His130, His158, Met159, Met162 and His194, as well as carbonyls of Lys131 and Lys195, are shown in red. (B) Space-filling representation of the same conformer showing the degree of residue conservation calculated with ConSurf. Conservation scores are arranged into nine groups with the corresponding colors ranging from cyan (most variable) to burgundy (most conserved). The numbering shown here is that of the UniProt entry BSU05790.

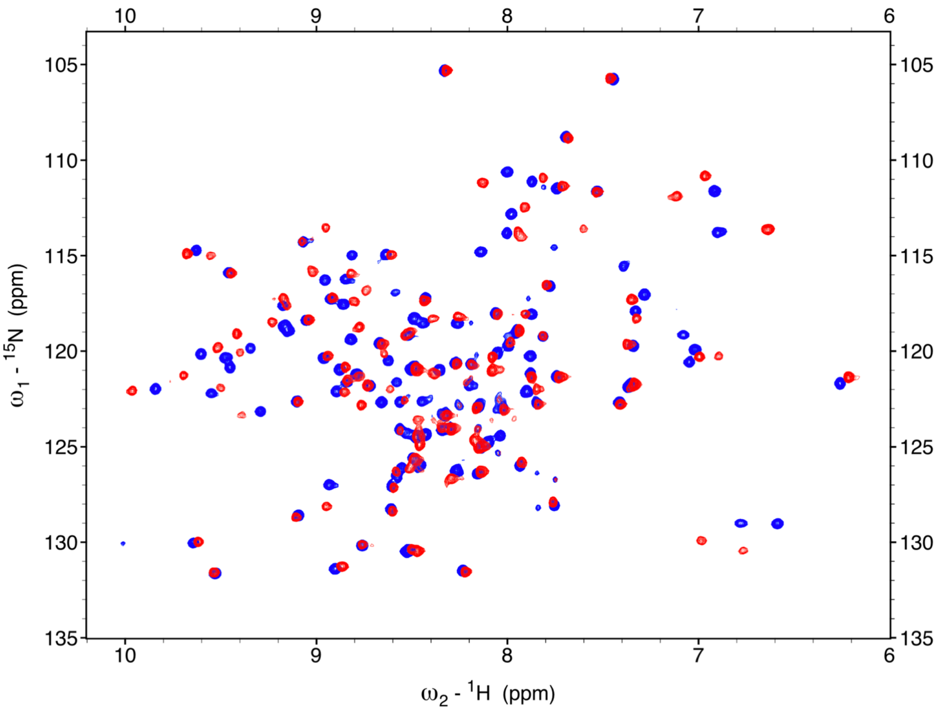


**Figure 8. Chemical shift perturbations of *B. subtilis* CopL due to $Cu^{1+}$ binding.**
Overlay of 600 MHz [$^{15}$N,$^{1}$H]-HSQC spectra of 0.3 mM apo-bsCopL-N (blue) and 0.3 mM holo-bsCopL-N with 6 mol/mol equivalents of $Cu^{1+}$ (red). The sequence-specific [$^{15}$N,$^{1}$H]-HSQC resonance assignments for apo-bsCopL-N are shown in Supplementary Figure S15.

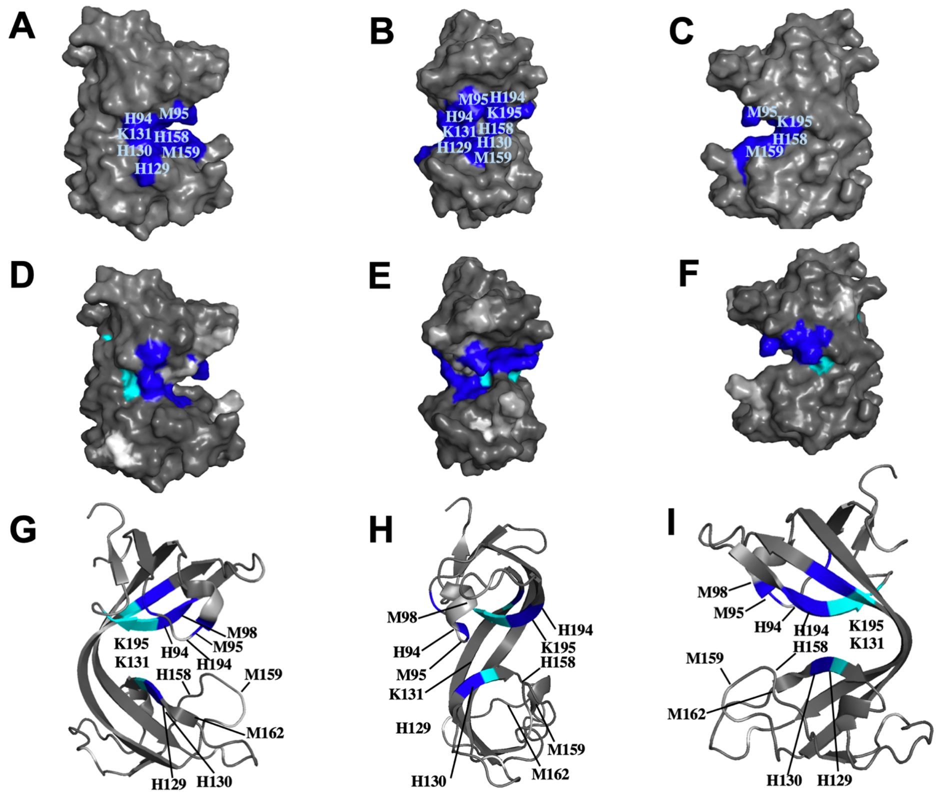


**Figure 9. $Cu^{1+}$ binding to *B. subtilis* CopL.**
(A-C). Surface molecular representation of *B. subtilis* CopL, in three orientations, showing the locations of conserved residues His94, Met95, Met98 (buried), His129, His130, Lys131, His158, Met159, Met162 (buried), His194, and Lys195, presumed to be involved in coordinating $Cu^{1+}$. Only residues that can be seen on the surface of the 3D structure are labeled. (D-F) Surface representation of *B. subtilis* CopL, in same three orientations, showing chemical shift perturbations due to $Cu^{1+}$-binding. Color code: dark blue, ($\Delta\delta_{NH} > 0.25$ ppm, *viz.,* Thr92, Met95, His130, His131, Met179, Val180, Asn193, His194, Lys195); Cyan, residues with $H^N$ resonances that are broadened due to $Cu^{1+}$ -binding (*viz*, Trp132, Tyr178, Trp196, Val197, and Thr198); light grey, residues with $H^N$ resonances which are absent in the [$^{15}N$,$^1H$]-HSQC spectrum of apo-CopL and not assigned (*viz* Lys 83, His94, Lys 96, Gly97, Lys160, Gly161, and Ser187), and white for proline residues which lack backbone amide protons (*viz*, Pro120 and Pro148). (G-I) Ribbon representation of *B. subtilis* CopL, in same three orientations, showing conformational perturbations due to $Cu^{1+}$-binding using the same color code as in panels D-F. In panels G - I, only the residues with $H^N$ resonances that are affected by $Cu^{1+}$-binding are labeled. The numbering shown here is that of the UniProt entry BSU05790.

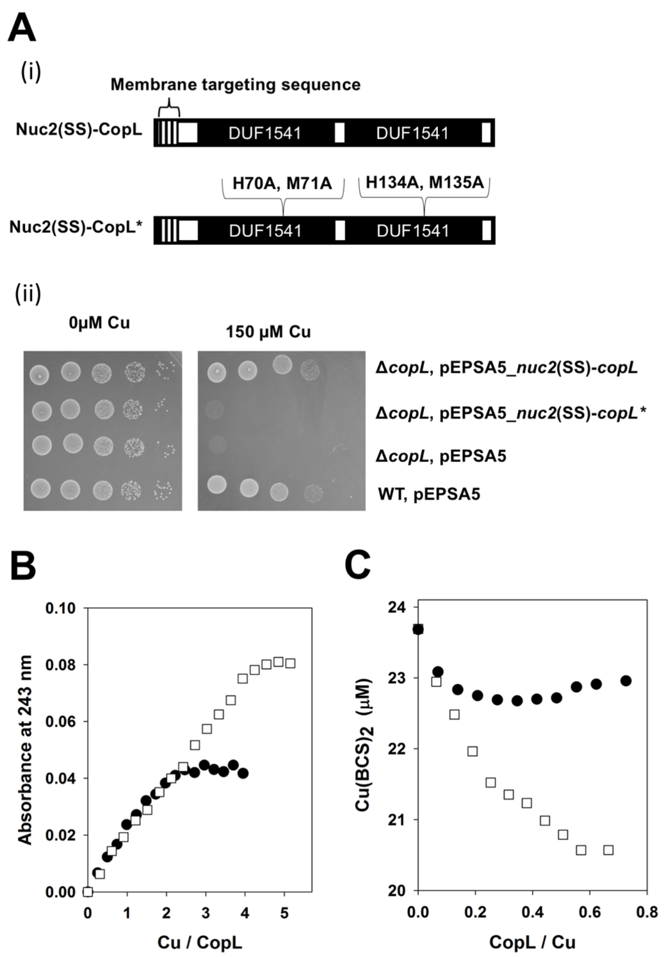


**Figure 10. Effective Cu binding is necessary for CopL to protect against Cu toxicity.** (A) The *copL** allele does not correct the Cu-sensitivity phenotype of a *S. aureus* Δ*copL* mutant. (i) Schematic of the *copL* and *copL** constructs utilized. (ii) The WT and Δ*copL* strains harboring pEPSA5, pEPSA5_*nuc2*(SS)-*copL*, or pEPSA5_*nuc2*(SS)-*copL** were serial diluted and spot plated on chemically defined media without and with 100 µM Cu. (B) The saCopL(T)* binds less $Cu^{1+}$ than saCopL(T). 12.5 µM apo-saCopL(T) or apo-saCopL(T)* were anaerobically titrated with $Cu^{1+}$. Binding was monitored by measuring absorbance at 243 nm using UV absorption spectroscopy. (C) saCopL(T)* has a lower affinity for $Cu^{1+}$ than saCopL(T). Solutions containing 0.5 mM BCS and 20 µM $Cu^{1+}$ were titrated with either apo-saCopL(T) or apo-saCopL(T)*. Copper binding to CopL was examined using BCS displacement by monitoring sample absorbance at 483 nm, which is the absorption maxima for the $Cu^{1+}$-BCS complex. The data for the saCopL(T) are also presented in Figure 6 and included here for comparison.

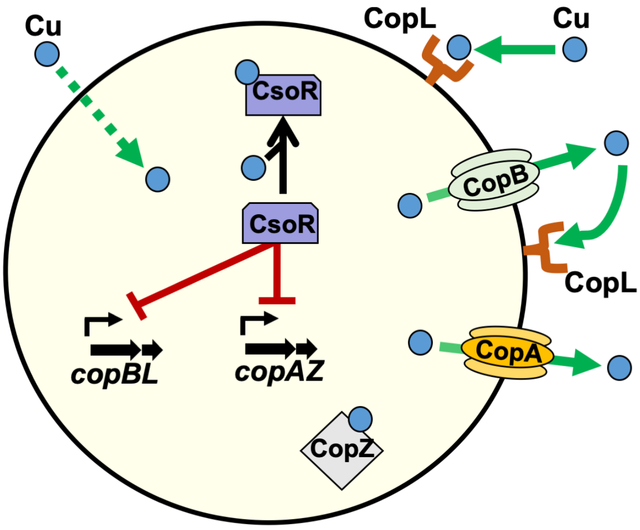


**Figure 11. Working model for copper homeostasis in *S. aureus*.**
The CsoR transcriptional regulator binds intracellular copper, leading to derepression of the *copAZ* and *copBL* operons. CopA and CopB are transmembrane copper-exporters. CopZ is a chaperone protein that binds copper and acts as a cytosolic buffer. CopL is a membrane-bound, surface-exposed, copper-binding lipoprotein. CopL likely functions in preventing copper uptake by binding extracellular Cu to prevent it from entering or re-entering the cell after export by CopB or CopA.

**The *copBL* operon protects *Staphylococcus aureus* from copper toxicity: CopL is an extracellular membrane-associated copper-binding protein**

Zuelay Rosario-Cruz, Alexander Eletsky, Nourhan S. Daigham, Hassan Al-Tameemi, G.V.T. Swapna, Peter C. Kahn, Thomas Szyperski, Gaetano T. Montelione and Jeffrey M. Boyd

*J. Biol. Chem. published online January 17, 2019*